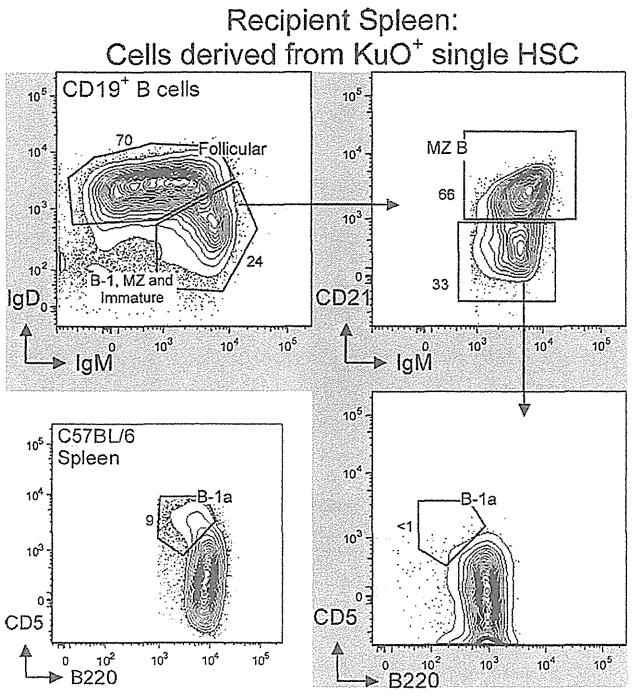

Fig. 3. Reconstitution of recipient spleen B cells after single HSC transfer. Individual HSCs were isolated from adult (9 wk) bone marrow (BM) of KuO$^+$ mice and injected i.v. to lethally irradiated C57BL/6 recipients. Recipient spleen was analyzed 27 wk after single HSC (KuO$^+$) transfer. Total HSC-derived B cells in recipient spleen were identified by the expression of CD19$^+$ and KuO$^+$. Sorted and transferred individual KuO$^+$ HSCs readily reconstituted follicular B-2 cells (IgD^{hi}, IgM^{lo}, and B220^{hi}), marginal zone B (MZ) cells (CD21^{hi}, IgD^{lo}, and IgM^{hi}), and immature B cells (IgM^{hi}, IgD^{lo}, CD21$^-$, and CD5$^-$) at appropriate proportions. However, sorted and transferred individual KuO$^+$ HSCs failed to reconstitute B-1a (CD5$^+$, B220^{lo}, and CD19^{hi}) in recipient spleen, even after 27 wk of HSC transplantation.

T cells in the earliest lymphoid development wave(s), whereas B-2 would colocate with αβ T cells.

The development of the hematopoietic system in man similarly changes with age (28). The differences between fetal/neonatal and adult erythroid development are well established. In addition, McCune et al. have shown that human fetal and adult T cells belong to distinct subsets originating from HSCs that are present in different stages during development (29). Moreover, they show that the fetal T-cell lineage is biased toward immune tolerance, providing a plausible mechanistic explanation for the unique tolerogenic properties of the immune system during ontogeny (29). Finally, findings from the de la Hera and Rothstein laboratories report phenotypic and functional shifts in the B-cell compartment during development (30–32) that, as in the mouse, distinguish the B-cell development pathway in children from the well-known adult pathway.

Interestingly, the findings discussed above were predicted by the "layered immune system" model proposed by our laboratory over two decades ago (13, 16). In essence, this model suggests that as species evolved, layers were added to the immune system to perform functions necessary for the survival of more advanced species. In addition, consistent with the idea that ontogeny recapitulates phylogeny, the model proposes that more advanced functions (e.g., affinity maturation) were associated with immune system components that evolved to be expressed later in development, when more diverse and directed functionality is required.

B-1 and B-2, with their specialized functions and their differential development, engendered this layered immune system model (13, 21). However, the proposed model generated more heat than light for many years, largely because better tools were needed to clearly define the developmental origins of B-1 and B-2. The HSC transfer data demonstrate clearly that adult BM contains HSCs that do not give rise to B-1a, but clearly give rise to B-2, MZ, and B-1b. Thus, B-1a emerges as a distinct developmental lineage whose early development, which occurs and is largely complete before the emergence of the B-cell lineages that predominate in adults, is consistent with the layered immune system model.

These findings have direct implications for BM human transplantation protocols (33). HSCs from adult BM have widely been considered to be capable of reconstituting all hematopoietic cells. However, data from both mouse and man now indicate that HSC populations in adult BM (and perhaps in cord blood) may be heterogeneous and may be limited with respect to the potential for regenerating the various hematopoietic cells present in adults (17, 34). If so, then technologies will have to be developed to enable the full reconstitution of the adult immune system.

Materials and Methods

Mice and Tissue Preparation. BALB/c (IgH^a allotype), CB.17 (IgH^b allotype), and RAG1$^{-/-}$ mice (8–10 wk old) were purchased from Jackson Labs or bred at the Stanford Medical School Animal Care Facility. C57BL/6-Ly5.2 and Ly5.1/Ly5.2-F$_1$ recipient mice (8–9 wk old) were bred at the Institute of Medical Science, University of Tokyo, Tokyo, Japan, and a transgenic mouse line expressing the fluorescent marker humanized Kusabira Orange (huKO) was a generous gift from Masafumi Onodera (National Center for Child Health and Development, Tokyo, Japan). All experiments were conducted with institutional animal care and use committee approval. PerC cells were harvested by injecting 7 mL of staining medium [deficient RPMI plus 3% (vol/vol) newborn calf serum] into PerC. Spleen was disrupted and resuspended to obtain single cell suspensions. BM from femurs and tibias was washed multiple times using a syringe to obtain single cell suspensions. All cell samples were filtered and resuspended at 25 × 10^6 cells/mL using custom

Table 2. B-cell subset reconstitution after in vivo cell transfer studies

Cells transferred to lethally irradiated recipients					Progeny B cells			
Source (reference)	Donor age	Isolation	Type	Phenotype	B-1a	B-1b	MZ	B-2
Yolk sac* (22)	E9–9.5	Culture*	Hemogenic endothelial cells	VE-cadherin$^+$ CD41$^-$	++	++	++	None
Yolk sac (24)	E12–13	Whole tissue	Total cells		+++	+++	+++	+++
Fetal liver (2, 11)	E13-prior birth	Whole tissue	Total cells		++	+++	(?)	+++
Neonatal BM (5)	2.5 wk	Bulk sort	HSC	KSL CD150$^+$	++	+++	(?)	+++
Adult BM	>8 wk	Single cell	HSC	KSL CD34$^-$CD150$^+$	None	++	+++	+++

The amount of reconstitution of each B-cell subset (B-1a, B-1b, marginal zone, and B-2) in lethally irradiated recipients is directly dependent on the source of donor cells used in these transfer studies.
*Isolated at indicated day and cultured for 5–11 d before transfer.

RPMI medium 1640 deficient in biotin, L-glutamine, phenol red, riboflavin, and sodium bicarbonate (Invitrogen).

FACS. Cell suspensions were preincubated with anti-CD16/CD32 mAb to block FcγRII/III and stained on ice for 30 min with the following fluorochrome-conjugated mAb in an 11-color staining combination: FITC-labeled anti-CD21 (7G6) or anti-Ig κ- and λ-light chains (187.1 and R26-46, respectively); PE-labeled anti-CD43 (S7) or anti-IgM^a (DS-1); PECy5-labeled anti-CD5 (53-7.3); PECy5.5-labeled anti-CD19 (1D3); PECy7-labeled anti-IgM (331); APC-labeled anti-B220 (RA3-6B2) or anti-CD23 (B3B4); Alexa700-labeled anti-IgD (11–28) or anti-IgM^b (AF6-78.25); APCCy7-labeled anti-CD19 (1D3), anti-B220 (RA3-6B2), or anti-CD11b (M1/70); Pacific Blue-labeled (Dump channel) anti-F4/80 (BM8), anti-Gr-1 (RB6-8C5), and anti-CD11b (M1/70); biotin-labeled anti-Ig κ- and λ-light chains (187.1 and R26-46, respectively) or anti-CD23 (B3B4). Cells were then washed and stained again on ice for 15 min with streptavidin Qdot 605 (Invitrogen) to reveal biotin-coupled antibodies. Antibodies were either purchased (Invitrogen and BD Pharmingen) or conjugated in our laboratory at Stanford University. After washing, stained cells were resuspended in 10 μg/mL propidium iodide (PI), idenitified on PE-Texas Red channel), to exclude dead cells (i.e., PI$^+$ cells). Cells were analyzed and sorted on Stanford FACS facility instruments (Becton Dickinson LSRII or FACSAria). Data were collected for 0.2–1 × 10^6 cells. Staining protocols were designed with CytoGenie software (Woodside Logic); data were analyzed with FlowJo software (TreeStar). To distinguish autofluorescent cells from cells expressing low levels of individual surface markers, we established upper thresholds for autofluorescence by staining samples with fluorescence-minus-one control stain sets in which a reagent for a channel of interest is omitted.

Sorting and Transfer of Single HSC. Total BM cells from 9-wk-old huKO transgenic mice were stained with biotin-labeled lineage markers mAb (anti-CD4, CD8, Gr-1, Ter-119, B220, and IL-7R) on ice for 30 min. Cells were then washed and stained again on ice for 90 min with the following fluorochrome-conjugated mAb: PECy7-labeled anti-CD117 (c-Kit 2B8); APC-labeled anti-CD150 (SLAM); Alexa700-labeled anti-CD34 (RAM34); Pacific Blue-labeled anti–Sca-1 (Ly-6A/E D7) and with streptavidin-APCCy7 to reveal biotin-coupled mAb. After washing, stained cells were resuspended in 10 μg/mL PI to exclude dead (PI$^+$) cells. KuO$^+$ HSCs were identified as Lin$^-$CD34$^{-/lo}$c-Kit$^+$Sca-1$^+$CD150$^+$ and individually sorted in 96-well plates. Individual KuO$^+$ HSCs were transferred i.v. to 80 lethally irradiated (two doses of 4.9 Gy delivered 4 h apart) C57BL/6 recipients along with 2 × 10^5 whole BM competitor cells from 8-wk-old Ly5.1/Ly5.2-F1 mice. After 30 wk, recipient PerC and spleen cells were harvested and KuO$^+$ HSC-derived B cells were analyzed as described above. BM-derived HSCs were sorted on a FACSAriaII (Becton Dickinson).

Chimerism. In this study, 80 mice received a single HSC i.v. along with 2 × 10^5 congenic BM cells. Recipient mice were bled monthly to check for the level of chimerism, i.e., percentage of immune cells derived from the single HSC (KuO$^+$) versus percentage of immune cells derived from the competitor congenic BM (KuO$^-$). A total of 17/80 recipient mice showed some level of chimerism in one, or all, hematopoietic lineages analyzed in blood (erythrocytes, platelets, myeloid cells, T cells, and B cells). Here, we chose to examine the five recipients that had chimerism in all hematopoietic lineages and yet had the highest chimerism in the B-cell compartment (10–80% of total B cells in blood derived from sorted KuO$^+$ HSCs). These reconstituted hematopoietic cells were still readily detectable in blood when the mice were killed and tissues (PerC and spleen) harvested at 30 wk posttransfer.

Note Added in Proof. While this manuscript was under review, Yuan et al. (35) reported that adult HSC can be reprogrammed to express the fetal HSC developmental profile, including the ability to develop into B-1a. The authors interpret these findings, as we interpret the HSC developmental difference reported here, as support for the Layered Immune System model that we first proposed in the late 1980s.

ACKNOWLEDGMENTS. We thank Megan Phillips for excellent technical help; P. Sadate-Ngatchou, Motohito Okabe, and Makoto Otsu for helpful discussion; Masafumi Onodera for providing huKO transgenic mice; and John Mantovani and Claudia Weber for administrative support. This work was supported by National Institutes of Health Grant AI076434 and by grants from the Japanese Ministry of Education, Culture, Sport, Science and Technology.

1. Spangrude GJ, Heimfeld S, Weissman IL (1988) Purification and characterization of mouse hematopoietic stem cells. *Science* 241:58–62.
2. Morrison SJ, Hemmati HD, Wandycz AM, Weissman IL (1995) The purification and characterization of fetal liver hematopoietic stem cells. *Proc Natl Acad Sci USA* 92: 10302–10306.
3. Cao YA, et al. (2004) Shifting foci of hematopoiesis during reconstitution from single stem cells. *Proc Natl Acad Sci USA* 101:221–226.
4. Lu R, Neff NF, Quake SR, Weissman IL (2011) Tracking single hematopoietic stem cells in vivo using high-throughput sequencing in conjunction with viral genetic barcoding. *Nat Biotechnol* 29:928–933.
5. Barber CL, Montecino-Rodriguez E, Dorshkind K (2011) Reduced production of B-1–specified common lymphoid progenitors results in diminished potential of adult marrow to generate B-1 cells. *Proc Natl Acad Sci USA* 108:13700–13704.
6. Barber CL, Montecino-Rodriguez E, Dorshkind K (2011) Developmental relationships between B-1 and B-2 progenitors. *Cell Cycle* 10(22):3810–3811.
7. Kantor AB, Stall AM, Adams S, Herzenberg LA, Herzenberg LA (1992) Differential development of progenitor activity for three B-cell lineages. *Proc Natl Acad Sci USA* 89:3320–3324.
8. Kantor AB, Stall AM, Adams S, Herzenberg LA, Herzenberg LA (1992) Adoptive transfer of murine B-cell lineages. *Ann N Y Acad Sci* 651:168–169.
9. Stall AM, Adams S, Herzenberg LA, Kantor AB (1992) Characteristics and development of the murine B-1b (Ly-1 B sister) cell population. *Ann N Y Acad Sci* 651:33–43.
10. Herzenberg LA, Kantor AB (1993) B-cell lineages exist in the mouse. *Immunol Today* 14:79–83, discussion 88–90.
11. Kantor AB, Herzenberg LA (1993) Origin of murine B cell lineages. *Annu Rev Immunol* 11:501–538.
12. Kantor AB, Stall AM, Adams S, Watanabe K, Herzenberg LA (1995) De novo development and self-replenishment of B cells. *Int Immunol* 7:55–68.
13. Herzenberg LA, Kantor AB, Herzenberg LA (1992) Layered evolution in the immune system. A model for the ontogeny and development of multiple lymphocyte lineages. *Ann N Y Acad Sci* 651:1–9.
14. Kim I, Saunders TL, Morrison SJ (2007) Sox17 dependence distinguishes the transcriptional regulation of fetal from adult hematopoietic stem cells. *Cell* 130:470–483.
15. He S, Kim I, Lim MS, Morrison SJ (2011) Sox17 expression confers self-renewal potential and fetal stem cell characteristics upon adult hematopoietic progenitors. *Genes Dev* 25:1613–1627.
16. Herzenberg LA, Herzenberg LA (1989) Toward a layered immune system. *Cell* 59:953–954.
17. Morita Y, Ema H, Nakauchi H (2010) Heterogeneity and hierarchy within the most primitive hematopoietic stem cell compartment. *J Exp Med* 207:1173–1182.
18. Hayakawa K, Hardy RR, Herzenberg LA, Herzenberg LA (1985) Progenitors for Ly-1 B cells are distinct from progenitors for other B cells. *J Exp Med* 161:1554–1568.
19. Lu LS, et al. (2002) Identification of a germ-line pro-B cell subset that distinguishes the fetal/neonatal from the adult B cell development pathway. *Proc Natl Acad Sci USA* 99:3007–3012.
20. Tung JW, Mrazek MD, Yang Y, Herzenberg LA, Herzenberg LA (2006) Phenotypically distinct B cell development pathways map to the three B cell lineages in the mouse. *Proc Natl Acad Sci USA* 103:6293–6298.
21. Tung JW, Herzenberg LA (2007) Unraveling B-1 progenitors. *Curr Opin Immunol* 19:150–155.
22. Montecino-Rodriguez E, Leathers H, Dorshkind K (2006) Identification of a B-1 B cell-specified progenitor. *Nat Immunol* 7:293–301.
23. Ghosn EE, Sadate-Ngatchou P, Yang Y, Herzenberg LA, Herzenberg LA (2011) Distinct progenitors for B-1 and B-2 cells are present in adult mouse spleen. *Proc Natl Acad Sci USA* 108:2879–2884.
24. Yoshimoto M, et al. (2011) Embryonic day 9 yolk sac and intra-embryonic hemogenic endothelium independently generate a B-1 and marginal zone progenitor lacking B-2 potential. *Proc Natl Acad Sci USA* 108:1468–1473.
25. Dorshkind K, Montecino-Rodriguez E (2007) Fetal B-cell lymphopoiesis and the emergence of B-1-cell potential. *Nat Rev Immunol* 7:213–219.
26. Samokhvalov IM, Samokhvalova NI, Nishikawa S (2007) Cell tracing shows the contribution of the yolk sac to adult haematopoiesis. *Nature* 446:1056–1061.
27. Havran WL, Allison JP (1988) Developmentally ordered appearance of thymocytes expressing different T-cell antigen receptors. *Nature* 335:443–445.
28. Mold JE, McCune JM (2011) At the crossroads between tolerance and aggression: Revisiting the "layered immune system" hypothesis. *Chimerism* 2:35–41.
29. Mold JE, et al. (2010) Fetal and adult hematopoietic stem cells give rise to distinct T cell lineages in humans. *Science* 330:1695–1699.
30. Sanz E, et al. (2010) Ordering human CD34+CD10-CD19+ pre/pro-B-cell and CD19- common lymphoid progenitor stages in two pro-B-cell development pathways. *Proc Natl Acad Sci USA* 107:5925–5930.
31. Griffin DO, Holodick NE, Rothstein TL (2011) Human B1 cells in umbilical cord and adult peripheral blood express the novel phenotype CD20+ CD27+ CD43+ CD70-. *J Exp Med* 208:67–80.
32. Griffin DO, Rothstein TL (2011) A small CD11b+ human B1 cell subpopulation stimulates T cells and is expanded in lupus. *J Exp Med* 208:2591–2598.
33. Czechowicz A, Weissman IL (2011) Purified hematopoietic stem cell transplantation: The next generation of blood and immune replacement. *Hematol Oncol Clin North Am* 25:75–87.
34. Beerman I, et al. (2010) Functionally distinct hematopoietic stem cells modulate hematopoietic lineage potential during aging by a mechanism of clonal expansion. *Proc Natl Acad Sci USA* 107:5465–5470.
35. Yuan J, Nguyen CK, Liu X, Kanellopoulou C, Muljo SA (2012) Lin28b reprograms adult bone marrow hematopoietic progenitors to mediate fetal-like lymphopoiesis. *Science*, 10.1126/science.1216557.

Cell

A Differentiation Checkpoint Limits Hematopoietic Stem Cell Self-Renewal in Response to DNA Damage

Jianwei Wang,[1] Qian Sun,[1,12] Yohei Morita,[1,12] Hong Jiang,[1] Alexander Groß,[2] André Lechel,[1] Kai Hildner,[5] Luis Miguel Guachalla,[1] Anne Gompf,[1] Daniel Hartmann,[1] Axel Schambach,[6] Torsten Wuestefeld,[7,8] Daniel Dauch,[7,8] Hubert Schrezenmeier,[3,11] Wolf-Karsten Hofmann,[9] Hiromitsu Nakauchi,[10] Zhenyu Ju,[4] Hans A. Kestler,[2] Lars Zender,[7,8] and K. Lenhard Rudolph[1,*]

[1]Institute of Molecular Medicine and Max-Planck-Research Department of Stem Cell Aging
[2]Research Group Bioinformatics and Systems Biology, Institute of Neural Information Processing
[3]Institute for Clinical Transfusion Medicine and Immunogenetics
University of Ulm, 89069 Ulm, Germany
[4]Institute of Aging Research, Hangzhou Normal University College of Medicine, Hangzhou, China
[5]Department of Medicine 1, Max Eder Research Group, University of Erlangen-Nürnberg, 91054 Erlangen, Germany
[6]Institute of Experimental Hematology, Hannover Medical School, 30625 Hannover, Germany
[7]Helmholtz Center for Infection Research, 38124 Braunschweig, Germany
[8]Department of Gastroenterology, Hepatology, and Endocrinology, Hannover Medical School, 30625 Hannover, Germany
[9]Department of Hematology and Oncology, Mannheim University Hospital, 68167 Mannheim, Germany
[10]Guest Professorship University of Ulm, Germany, Centre for Stem Cell Biology and Regenerative Medicine, Institute of Medical Science, University of Tokyo, and Japan Science and Technology Agency, ERATO, Tokyo 108-8639, Japan
[11]German Red Cross Blood Transfusion Service Baden-Wurttemberg-Hessen, D-76530 Baden, Germany
[12]These authors contributed equally to this work
*Correspondence: klrudolph@fli-leibniz.de
DOI 10.1016/j.cell.2012.01.040

SUMMARY

Checkpoints that limit stem cell self-renewal in response to DNA damage can contribute to cancer protection but may also promote tissue aging. Molecular components that control stem cell responses to DNA damage remain to be delineated. Using in vivo RNAi screens, we identified basic leucine zipper transcription factor, ATF-like (BATF) as a major component limiting self-renewal of hematopoietic stem cells (HSCs) in response to telomere dysfunction and γ-irradiation. DNA damage induces BATF in a G-CSF/STAT3-dependent manner resulting in lymphoid differentiation of HSCs. BATF deletion improves HSC self-renewal and function in response to γ-irradiation or telomere shortening but results in accumulation of DNA damage in HSCs. Analysis of bone marrow from patients with myelodysplastic syndrome supports the conclusion that DNA damage-dependent induction of BATF is conserved in human HSCs. Together, these results provide experimental evidence that a BATF-dependent differentiation checkpoint limits self-renewal of HSCs in response to DNA damage.

INTRODUCTION

An age-dependent decline in stem cell function occurs in various tissues and this decline contributes to impairments in tissue homeostasis during aging (Rando 2006, Sharpless and DePinho 2007). On the molecular level, there is experimental evidence that the accumulation of DNA damage can accelerate aging in mouse models and human progeria syndromes (Rudolph et al., 1999, Hoeijmakers 2009, Sahin and DePinho 2010). An age-dependent accumulation of DNA damage occurs in tissue stem cells (Rossi et al., 2007, Rübe et al., 2011). DNA damage checkpoints that limit the function of aging stem cells remain to be delineated.

Unbiased, functional genomic approaches can be conducted at stem cell level (Hope et al., 2010) and studies on carcinogenesis demonstrated the power of such approaches to discover tumor suppressor checkpoints (Zender et al., 2008). Tumor suppressor checkpoints can also limit the regenerative capacity of tissues during aging, e.g., p53, p16, p21 (Chin et al., 1999, Signer et al., 2008, Janzen et al., 2006, Liu et al., 2011, Molofsky et al., 2006, Nishino et al., 2008, Choudhury et al., 2007, Sharpless and DePinho 2007). This dual role of checkpoint genes in cancer protection and aging could also be relevant at stem cell level (Pelicci 2004, Beausejour and Campisi 2006, Sharpless and DePinho 2007). It is possible that DNA damage checkpoints protect from stem cell-derived cancer but contribute to impairments in stem cell function during aging.

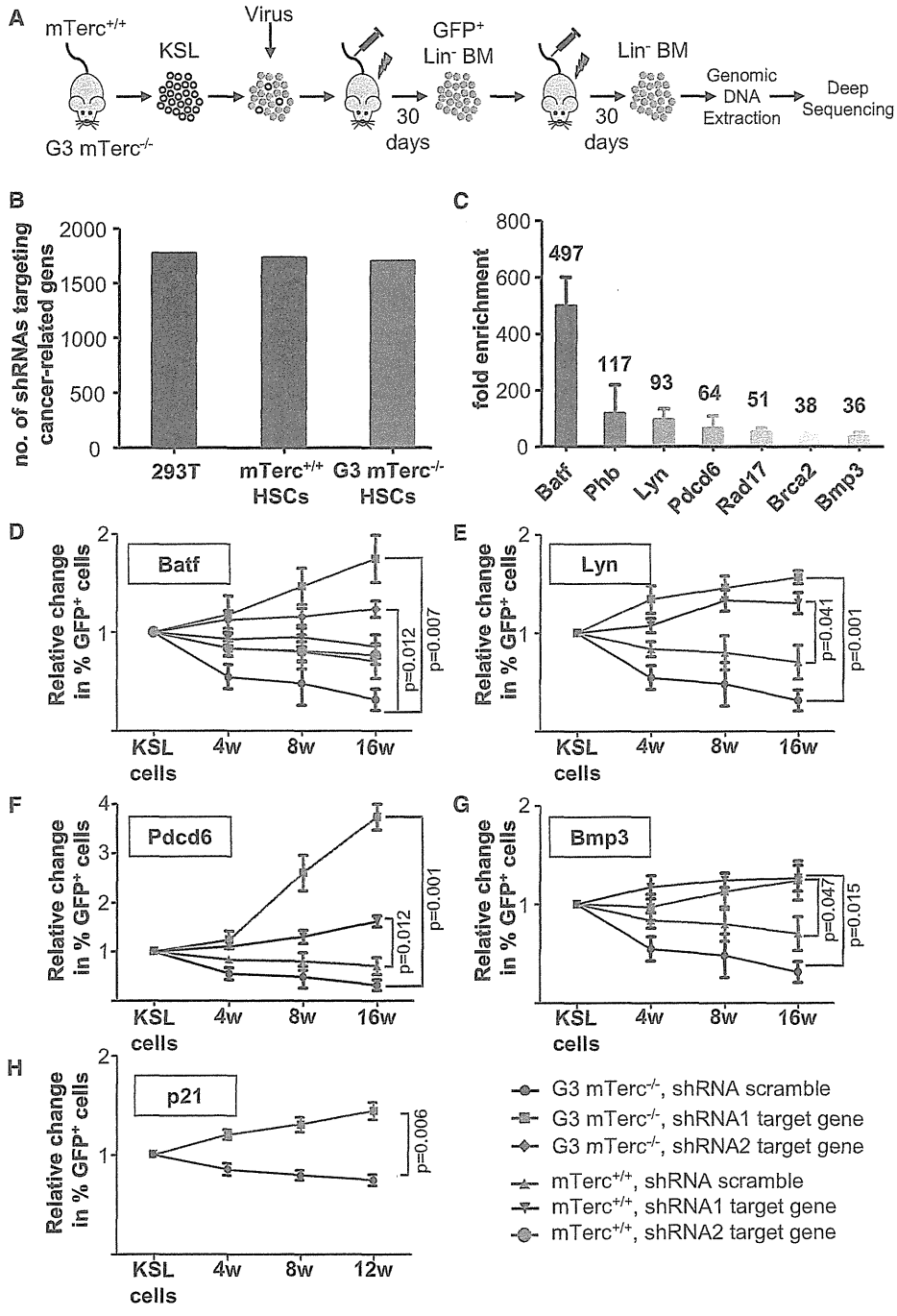

Figure 1. In Vivo RNAi Screening Identifies Candidate Checkpoints in Telomere Dysfunctional HSCs

(A–C) Freshly isolated KSL cells from 3 month old *mTerc*$^{+/+}$ and G3 *mTerc*$^{-/-}$ mice (n = 24 mice per group) were infected with a pool of lentiviruses and were transplanted for 2 rounds into lethally irradiated recipients (n = 24 mice per group) along with noninfected KSL cells from the same culture. Four weeks later, Lin$^-$ BM cells were analyzed by deep sequencing.

(B) The histogram depicts the numbers of shRNAs that were detected by deep sequencing in virus producer cells and Lin$^-$ bone marrow cells from secondary recipients.

(C) Histogram showing the strongest selected shRNAs in G3 *mTerc*$^{-/-}$ Lin$^-$ cells compared to *mTerc*$^{+/+}$ Lin$^-$ cells.

(D–H) Freshly isolated KSL cells from *mTerc*$^{+/+}$ or G3 *mTerc*$^{-/-}$ mice (n = 8 donors per group) were infected with single shRNA constructs targeting candidate genes or with a scrambled shRNA control. The infection rate was 22%–50% and was normalized to 1. Infected cells were transplanted into

Telomere shortening represents a cell intrinsic mechanism contributing to the accumulation of DNA damage in aging cells (d'Adda di Fagagna et al., 2003). Critically short telomeres lose capping function at chromosome ends and induce DNA damage responses (Chin et al., 1999, d'Adda di Fagagna et al., 2003) that lead to induction of cell cycle arrest or apoptosis (Lee et al., 1998, Wright and Shay, 1992). Studies on late generation telomerase knockout mice revealed experimental evidence that telomere dysfunction impairs somatic stem cell maintenance and function (Wong et al., 2003; Allsopp et al., 2003) by induction of DNA damage checkpoints (Choudhury et al., 2007, Schaetzlein et al., 2007).

Hematopoietic stem cells (HSCs) represent one of the best-studied somatic stem cell systems. HSC aging is characterized by a decline in the repopulation capacity and skewed differentiation (Morrison et al., 1996, Sudo et al., 2000, Rossi et al., 2005) likely contributing to the age-associated defects in immune functions (Wang et al., 2011, Rossi et al., 2008, Linton and Dorshkind 2004). The molecular pathways that impair repopulation capacity and differentiation of aging HSCs are largely unknown.

Here, we conducted a small in vivo RNAi screen to identify molecular pathways inhibiting HSC function in response to telomere dysfunction. The study provides experimental evidence for a differentiation checkpoint limiting self-renewal of HSCs in response to DNA damage. This checkpoint appears to be conserved in human HSCs and could represent a major target to prevent functional decline and the evolution of malignancies in the aging hematopoietic system.

RESULTS

In Vivo RNAi Screening Identifies Target Genes Rescuing the Repopulation Capacity of Telomere Dysfunctional Stem Cells

An in vivo RNAi screen was conducted on transplanted HSCs from telomere dysfunctional mice (third generation telomerase knockout: G3 *mTerc*$^{-/-}$) compared to wild-type mice with long telomere reserves (*mTerc*$^{+/+}$, n = 24 donors per group, Figure 1A). The RNAi library was derived from a recently published set of shRNAs targeting 947 cancer related genes (Bric et al., 2009, Figure S1, Table S1). cKit^{+} Sca1^{+} lineage^{-} (KSL) cells from the donor cohorts were pooled and infected with the shRNA pool (multiplicity of infection: 10–30, transduction efficiency: 82%–84%). On average, each shRNA was infected in approximately 500 KSL cells. Virally transduced KSL cells were transplanted for two consecutive rounds into lethally irradiated recipients. Four weeks later, hematopoietic cells were isolated and deep sequencing revealed that the vast majority of shRNAs were still present in hematopoietic cells (Figure 1B) indicating that imbalances in the prevalence of individual shRNAs did not occur because of the random loss of shRNAs.

Seven shRNAs were strongly selected in recipients transplanted with G3 *mTerc*$^{-/-}$ HSCs compared to recipients of *mTerc*$^{+/+}$ HSCs (Figure 1C, Table S2). Single construct experiments showed that 4 out of 7 candidate shRNAs were positively selected in transplanted G3 *mTerc*$^{-/-}$ HSCs (Figures 1D–1G). All of these shRNAs exhibited a good knockdown efficiency of target genes on mRNA level (Figure S1B, Table S3). Three of the shRNAs also showed a positive selection in primary recipients transplanted with *mTerc*$^{+/+}$ hematopoietic cells albeit less pronounced compared to G3 *mTerc*$^{-/-}$ HSCs (Figures 1E–1G).

The strongest selected shRNAs in G3 *mTerc*$^{-/-}$ hematopoietic cells (497-fold enriched compared to *mTerc*$^{+/+}$ hematopoietic cells) targeted the "Basic leucine zipper transcription factor, ATF-like," also known as *Batf* (Dorsey et al., 1995, Figure 1C). Two independent shRNAs targeting *Batf* had no measurable effect on *mTerc*$^{+/+}$ hematopoietic cells but were strongly selected in transplanted G3 *mTerc*$^{-/-}$ hematopoietic cells correlating with knockdown efficiency of the 2 shRNAs (Figure S1B, Figure 1D). Previous studies showed that *p21* deletion rescues the function of telomere dysfunctional HSCs (Choudhury et al., 2007). shRNA mediated knockdown of *p21* shRNA was similarly effective in rescuing the repopulation capacity of telomere dysfunctional KSL cells compared to *Batf* knockdown (Figures 1D and 1H). Among other shRNAs in the RNAi library that targeted DNA damage checkpoint genes (*Atm*, *Gadd45a* and *Gadd45 g*, *Caspase 3*, *Rad17*, a.o.), the *Batf* shRNA was most strongest selected in hematopoietic cells from G3 *mTerc*$^{-/-}$ mice compared to *mTerc*$^{+/+}$ mice (Table S4).

Batf Deletion Improves Self-Renewal but Increases DNA Damage Accumulation of HSCs in Response to Telomere Dysfunction or γ-Irradiation

Chimeric bone marrow (BM) from primary recipients that were transplanted with shRNA *Batf* infected along with noninfected KSL cells (Figure 1D) was serially transplanted into secondary and tertiary recipients. *Batf* knockdown was not selected in serially transplanted *mTerc*$^{+/+}$ BM, but exhibited a strong, positive selection in serially transplanted G3 *mTerc*$^{-/-}$ BM (Figure 2A). Purified *Batf* shRNA infected G3 *mTerc*$^{-/-}$ BM cells (5x 10^{6} GFP^{+} cells) rescued lethally irradiated tertiary recipients, whereas vector control infected BM cells from the same donors exhausted at this stage (Figure 2B). These results indicated that *Batf* knockdown improved self-renewal of G3 *mTerc*$^{-/-}$ HSCs. In line with this interpretation, shRNA mediated knockdown of *Batf* rescued HSC numbers in long-term engrafted primary (Figure 2C) and secondary recipients of G3 *mTerc*$^{-/-}$ hematopoietic cells (data not shown). Control experiments confirmed that HSC self-renewal was compromised in aging G3 *mTerc*$^{-/-}$ mice but not in G1 *mTerc*$^{-/-}$ mice indicating that telomere shortening rather than *mTerc* gene status by itself limited HSC self-renewal (Figure S2A). Competitive transplantation of 200 or 400 highly purified shRNA infected HSCs (CD34^{-}KSL) from primary recipients confirmed that *Batf* knockdown improved multilineage repopulation capacity of G3 *mTerc*$^{-/-}$ HSCs (Figure 2D, Figure S2B). Telomere length analysis by quantitative

lethally irradiated recipients along with noninfected cells from the same culture (n = 3 recipients for each group). The histograms depict changes in peripheral blood chimerism of infected cells (GFP-positive) in primary recipients at the indicated time points after transplantation. Values are shown as mean ± SEM.

See Figure S1 and Table S1, Table S2, Table S3, and Table S4.

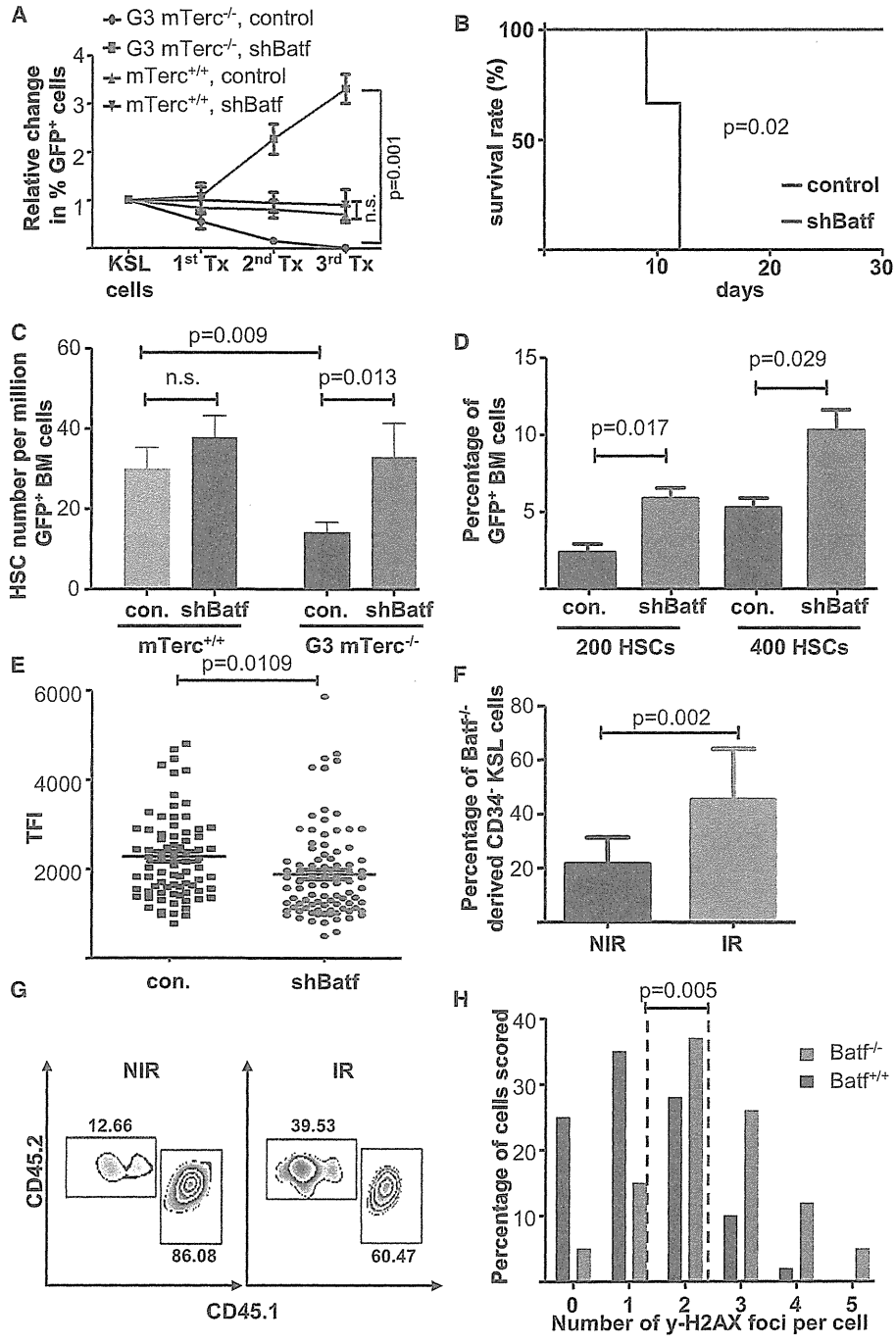

Figure 2. *Batf* Deletion Improves Self-Renewal but Increases DNA Damage Accumulation of HSCs in Response to Telomere Dysfunction or γ-Irradiation

(A–E) *Batf* shRNA and scrambled shRNA infected KSL cells of G3 $mTerc^{-/-}$ and $mTerc^{+/+}$ mice were transplanted into lethally irradiated recipients along with noninfected KSL cells. shRNA expressing lentiviruses coexpressed GFP. (A) Bone marrow (BM) of primary recipients was serially transplanted. The histogram shows changes in peripheral blood chimerism, 1 month after transplantation at the indicated round of serial transplantation. (B) In the 3rd round of serial transplantation 5×10^6 purified, infected BM cells were transplanted into lethally irradiated mice. The Kaplan Meier histogram depicts survival rates of recipients of *Batf* shRNA or scrambled shRNA infected G3 $mTerc^{-/-}$ bone marrow cells (n = 3 mice per group). (C) The histogram shows the numbers of HSCs ($CD34^-KSL$ cells) in GFP^+ BM cells of long-term engrafted (4 months after transplantation), primary recipients (n = 5 mice per group). (D) Purified HSCs (200 or 400 $CD34^-KSL$ cells) from primary recipients were transplanted into lethally irradiated recipients together with 500,000 competitor cells (total BM). The histogram shows the

fluorescence in situ hybridization (qFISH) showed that *Batf* deficiency prolonged maintenance of HSC with shortened telomeres (Figure 2E).

Bone marrow cells of *Batf* knockout mice ($Batf^{-/-}$) and wild-type mice ($Batf^{+/+}$) were transplanted into lethally irradiated recipients along with $Batf^{+/+}$ competitor cells. When primary recipients were exposed to a single dose of 4 Gy γ-irradiation, $Batf^{-/-}$ HSCs were positively selected (Figures 2F and 2G). Immunofluorescence staining against γH2AX (a marker of DNA breaks) indicated that *Batf* deficiency prolonged maintenance of HSCs carrying DNA damage (Figure 2H).

Together, these data indicated that *Batf* deletion or knockdown can improve the maintenance and function of HSCs in the context of telomere dysfunction or γ-irradiation but this rescue results in an accumulation of DNA damage and telomere shortening in the HSC pool. This conclusion was further supported by an analysis of the effects of *Batf* knockdown on hematopoietic progenitor cells. Specifically, shRNA-mediated knockdown of *Batf* rescued the impaired capacity of G3 $mTerc^{-/-}$ HSCs to generate multipotent progenitor cells (MPPs, p = 0.001, Figure S2C and S2F) and common myeloid progenitors (CMPs, p = 0.007, Figures S2D and S2F). *Batf* knockdown had minor effects on the generation of MPPs or CMPs in $mTerc^{+/+}$ HSC recipients (Figures S2C, S2D, and S2F). *Batf*-knockdown reduced the number of common lymphoid progenitors (CLPs) in recipients of both $mTerc^{+/+}$ and G3 $mTerc^{-/-}$ HSCs (Figures S2E and S2F). These data suggested that *Batf* could contribute to early stages of lymphoid lineage differentiation of HSCs. An alternative explanation indicated that *Batf* was required for survival of CLPs. In agreement with this interpretation, ex vivo infection of freshly purified CLPs from wild-type mice revealed that *Batf* knockdown impaired the survival of cultured CLPs (Figure S3A). Along with these data on impaired CLP formation/maintenance, recipients of *Batf* shRNA-infected HSCs exhibited a skewing in HSC differentiation resulting in increased myelopoiesis and decreased lymphopoiesis compared to recipients of scrambled shRNA infected HSCs (Figures S3B–S3D). Transplantation of *Batf* shRNA versus scrambled shRNA targeted CMPs showed that *Batf* knockdown did not induce self-renewal of CMPs (n = 5 mice per group, Figure S3E). These data support the conclusion that *Batf* knockdown rescued the repopulation capacity of G3 $mTerc^{-/-}$ HSCs rather than self-renewal of CMPs.

Batf Upregulation Impairs HSC Function in Response to Aging and DNA Damage

mRNA annalysis of freshly purified HSCs and hematopoietic progenitor cells from 3- and 12-month-old mice revealed that *Batf* mRNA expression was upregulated in hematopoietic progenitor cells (Figure 3A) as well as in long-term HSCs (Figure 3B) of G3 $mTerc^{-/-}$ mice compared to $mTerc^{+/+}$ mice. In both cohorts, an age-dependent induction of *Batf* mRNA levels was observed in HSCs (Figure 3B) possibly reflecting the increasing levels of DNA damage in aging HSCs (Rossi et al., 2007). On protein level, increased expression of BATF was seen in hematopoietic progenitor cells (KSL) and HSCs ($CD34^-$KSL) of G3 $mTerc^{-/-}$ mice compared to $mTerc^{+/+}$ mice (Figures 3C and 3D). Again, there was an age-dependent increase in both cohorts (Figure 3C).

Batf mRNA expression was also measured in freshly isolated HSCs from $mTerc^{+/+}$ mice at different time points after 4 Gy whole body γ-irradiation (IR). There was a significant induction of *Batf* mRNA expression from 6-48 hr after IR (Figure 3E, n = 3 mice per group). Irradiation-induced BATF expression was confirmed on protein level in freshly isolated HSCs (Figure 3F). *Batf*–cDNA expression experiments demonstrated that overexpression of *Batf* limited the repopulation capacity of HSCs (Figure S4A, Figure 3G,H).

G-CSF/STAT3-Dependent but p53-Independent Upregulation of BATF in HSCs in Response to DNA Damage

An analysis of BATF protein expression in freshly isolated Lin^- cells of γ-irradiated (4Gy) and nonirradiated *Trp53* knockout mice ($Trp53^{-/-}$) revealed that DNA damage-induced expression of BATF was p53-independent (Figure 4A). Previous studies suggested that STAT3-dependent upregulation of BATF induces differentiation of murine leukemia cells (Senga et al., 2002) and G-CSF can activate STAT3 (Tian et al., 1994). An analysis of BATF protein expression in Lin^- cells of nonirradiated and irradiated *G-Csf* knockout mice ($G\text{-}Csf^{-/-}$) and control mice ($G\text{-}Csf^{+/-}$) revealed that the induction of BATF in response to γ-irradiation was G-CSF-dependent (Figure 4B). Cell culture experiments showed that stimulation with G-CSF-induced BATF protein levels in freshly isolated hematopoietic cells (Lin^-) from wild-type mice and this induction was strongly STAT3-dependent (Figure 4C, Figure S4B). Transplantation of shRNA-transduced G3 $mTerc^{-/-}$ KSL cells showed that *Stat3* knockdown rescued the repopulation capacity of G3 $mTerc^{-/-}$ KSL cells (Figure 4D, $p < 0.001$). Together, these experiments indicated that STAT3/G-CSF-dependent upregulation of BATF impairs the self-renewal of HSCs in response to DNA damage.

DNA Damage Induces BATF-Dependent Lymphoid Differentiation of HSCs

BATF was implicated in the differentiation of peripheral lymphocytes (Betz et al., 2010, Schraml et al., 2009). Here, the mRNA

percentage of test donor-derived bone marrow cells 3 months after transplantation (n = 5 recipients per group). (E) Telomere length was analyzed by qFISH in purified HSCs ($CD34^-$KSL cells) from secondary recipients, 12 weeks after transplantation. The dot blot shows the distribution of telomere fluorescence intensities (TFI) over all analyzed nuclei. Lines depict mean values.

(F–H) Total BM of $Batf^{-/-}$ mice (CD45.2) was transplanted into 20 lethally irradiated recipients together with $Batf^{+/+}$ competitor cells (CD45.1). One month after transplantation, 10 recipients were γ-irradiated with 4Gy, 10 remained nonirradiated. Bone marrow of recipient mice was analyzed 2 months later. (F) The histogram depicts changes in the percentage of $Batf^{-/-}$ $CD34^-$KSL cell (CD45.2) in nonirradiate (NIR) versus irradiate (IR) recipients. (G) Representative blots from flow cytometry. (H) The histogram depicts the percentage of purified HSCs ($CD34^-$KSL) showing the indicated number of γH2AX foci per cell in immunofluorescence staining. The dotted line represents the mean value. (A,C,D,E) Values are shown as mean ± SEM.

See Extended Experimental Procedures and Figure S2 and Figure S3.

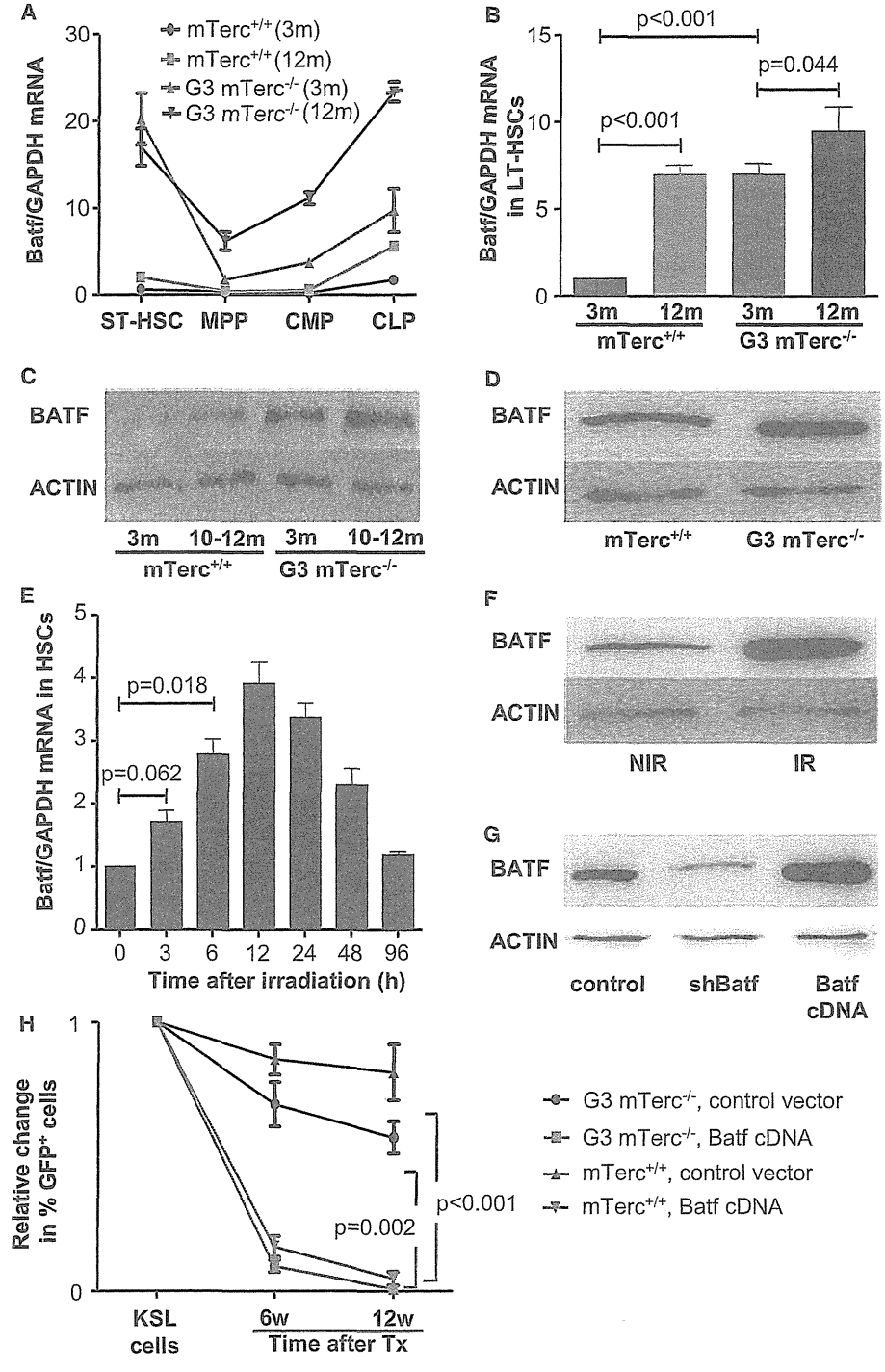

Figure 3. *Batf* **Upregulation Impairs HSC Function in Response to Aging and DNA Damage**

(A and B) The histograms show the mRNA expression of *Batf* relative to *Gapdh* in freshly purified progenitor cells from 3 and 12 month old *mTerc*$^{+/+}$ and G3 *mTerc*$^{-/-}$ mice in: (A) short-term hematopoietic stem cells (ST-HSCs: CD34^{+}Flt3^{-} KSL), multipotent progenitor cells (MPPs: CD34^{+}, Flt3^{+}, KSL), common myeloid progenitor cells (CMPs: Lin^{-}, Sca-1^{-}, c-Kit^{+}, CD34^{+}, CD16/32^{lo}), and common lymphoid progenitor cells (CLPs: Lin^{-}, Sca-1^{lo}, c-Kit^{lo}, IL7R^{+}, Flt3^{+}); (B) long-term HSCs (CD34^{-} Flt3^{-} KSL), (n = 3 mice per group; data are shown as mean; error bar represent SEM).

(C) Representative Western blot showing expression of BATF in freshly isolated hematopoietic progenitor cells (KSL) of 3 and 10-12 month old G3 *mTerc*$^{-/-}$ and *mTerc*$^{+/+}$ mice (n = 3 mice per group).

expression of lymphoid and myeloid marker genes that carry putative AP1-binding sides in the promoters, was measured in purified HSCs from 10-12 month old *mTerc*$^{+/+}$ and G3 *mTerc*$^{-/-}$ mice (Figures 5A–5C, Table S5). Telomere dysfunction and γ-irradiation was associated with a significant induction of genes associated with lymphoid differentiation and an inhibition of genes associated with myeloid differentiation (Figures 5A–5C, n = 3 mice per group). Freshly isolated G3 *mTerc*$^{-/-}$ HSCs were transduced with *Batf* shRNA or scrambled shRNA. Targeted HSCs were transplanted into wild-type recipients and re-isolated 4 months after transplantation. qPCR showed that the knockdown of *Batf* reverted the induction of lymphoid differentiation in G3 *mTerc*$^{-/-}$ HSCs (Figure 5C).

Interleukin-7-receptor (IL7R) knockin mice express Cre-recombinase under the endogenous IL7R promoter. When crossed to Cre-inducible reporter mice (e.g., Rosa26-lox-stop-lox-YFP), activation of the IL7R marks the onset of lymphoid differentiation by inducing reporter gene expression. It was shown that IL7R-reporter gene is not expressed at HSC level but gets activated during lymphoid differentiation at CLP level (Schlenner et al., 2010). Here, a significant induction of IL7R-reporter activity was detected 12 hr after 4Gy γ-irradiation in HSCs (CD34$^-$KSL) compared to nonirradiated mice (Figure S4C).

The CD150 marker (Kiel et al., 2005) can subdivide CD34$^-$KSL cells into myeloid competent HSCs (expressing high levels of CD150 = CD150^{hi}) and lymphoid competent HSCs (expressing low levels of CD150 = CD150^{lo}, Morita et al., 2010, Beerman et al., 2010). CD150-negative CD34$^-$KSL cells were not included in our analysis since these cells may not represent true stem cells (Kiel et al., 2008). Analyzing HSCs in response to γ-irradiation revealed a significant induction of IL7R-reporter activity in CD150^{lo} HSCs and to a much smaller extend in CD150^{hi} HSCs (Figures 5D and 5E) suggesting that lymphoid competent HSCs were more sensitive to DNA damage-induced lymphoid differentiation.

CD150^{hi} and CD150^{lo} HSCs of irradiated donor mice were separated according to the induction of IL7R-reporter and re-transplanted into lethally irradiated mice along with competitor cells. Il7R-reporter negative HSCs maintained some long-term, multilineage engraftment capacity, whereas IL7R-positive HSCs had lost this capacity (Figure S4D). Multilineage analysis revealed that IL7R+ HSCs differentiated into lymphoid cells (Figures S4E and S4F). Together, these data indicated that irradiation induces lymphoid differentiation thereby limiting the functional capacity of HSCs. Irradiation of long-term recipients of *Batf* shRNA or scrambled shRNA infected KSL cells from IL7R-reporter mice revealed that DNA damage-induced lymphoid differentiation of CD150^{lo} HSCs was BATF-dependent (Figures 5D and 5F).

IL7R-reporter induction was also analyzed ex vivo in freshly isolated, highly purified HSCs that were cocultured on OP9 feeder cells to foster lymphoid differentiation if present. Irradiation-induced lymphoid differentiation in 13.7 ± 1.21% of CD150^{hi} HSCs (Figures 5G and 5H) and in 52% of CD150^{lo} HSCs (Figure 5I). Since the percentage of contaminating lymphoid competent progenitor was significantly lower in both HSC compartments (0% in CD150^{hi} HSCs, 28% in CD150^{lo} HSC, Figure S4G). Specifically, recent studies revealed that 35%–45% of CD34-KSL cells represent 'true stem cells' exhibiting long-term, multilineage engraftment in single cell transplantation assays (Morita et al., 2010). However, this assay likely underestimates the percentage of 'true stem cells', since the seeding efficiency in single cell transplantation experiments is limited and only 50%–80% of the transplanted cells engraft. Here, we analyzed the cellular composition of myeloid competent HSCs (CD150^{hi}CD34$^-$KSL cells) that engraft in single cell transplantation assay. This population contains 68% 'true HSCs' (showing long-term multilineage engraftment) and 32% myeloid-restricted progenitor cells (showing only transient, myeloid-restricted engraftment) but no lymphoid competent progenitor cells (Figure S4G). The population of lymphoid competent HSCs (CD150^{lo}CD34$^-$KSL cells) that engraft in single cell transplantation assays contains 43% 'true HSCS' (showing long-term, multilineage engraftment), 28.5% of multipotent progenitor cells (MPPs, showing transient multilineage engraftment) and 28.5% myeloid-restricted progenitor cells (showing transient, myeloid-restricted engraftment) (Figure S4G). Control experiments verified that irradiation does not induce lymphoid differentiation of myeloid-restricted progenitor cells (Figure S4H). Together, these data demonstrated that irradiation-induced lymphoid differentiation affected 'true HSC' within both HSC populations.

Isolation of HSCs from recipients that were transplanted with shRNA infected HSCs revealed that *Batf* knockdown completely prevented DNA damage-induced activation of IL7R-reporter in freshly isolated CD150^{lo} HSCs under ex vivo culture conditions (Figures 5J and JK). A series of control experiments excluded that significant numbers of HSCs changed surface markers or that significant numbers of lymphoid progenitor cells moved into the population of surface marker defined HSCs at the investigated time points after DNA damage induction (Figure S5).

(D) Representative Western blot showing expression of BATF in freshly isolated HSCs (CD34$^-$KSL) from bone marrow of 10-12 month old G3 *mTerc*$^{-/-}$ and *mTerc*$^{+/+}$ mice (n = 5 mice per group).

(E) The histogram shows the mRNA expression of *Batf* relative to *Gapdh* in freshly isolated HSCs (CD34$^-$KSL) from bone marrow of 3 month old *mTerc*$^{+/+}$ mice at the indicated time points after γ-irradiation (4 Gy, n = 3 mice per time point).

(F) Representative Western blot showing expression of Batf in freshly isolated hematopoietic stem cells (CD34$^-$ KSL) from bone marrow of 10-12 month old *mTerc*$^{+/+}$ mice with or without γ-irradiation (4Gy, 12 hr after IR, n = 5 mice per group).

(G) Representative Western blot showing expression of BATF in freshly isolated, Lin$^-$ BM cells, 5 weeks after transplantation of shRNA-*Batf*, cDNA-*Batf* or scrambled shRNA transduced KSL cells from *mTerc*$^{+/+}$ mice.

(H) *Batf*-cDNA or empty vector infected KSL cells were transplanted along with noninfected cells into lethally irradiated recipients. The infection efficiency was 40%–50% and was normalized to 1. The histogram depicts changes in peripheral blood chimerisms of infected cells (GFP-positive) in primary recipients at the indicated time points after transplantation (n = 3 recipients per group; data are shown as mean ± SEM).

See Figure S4A.

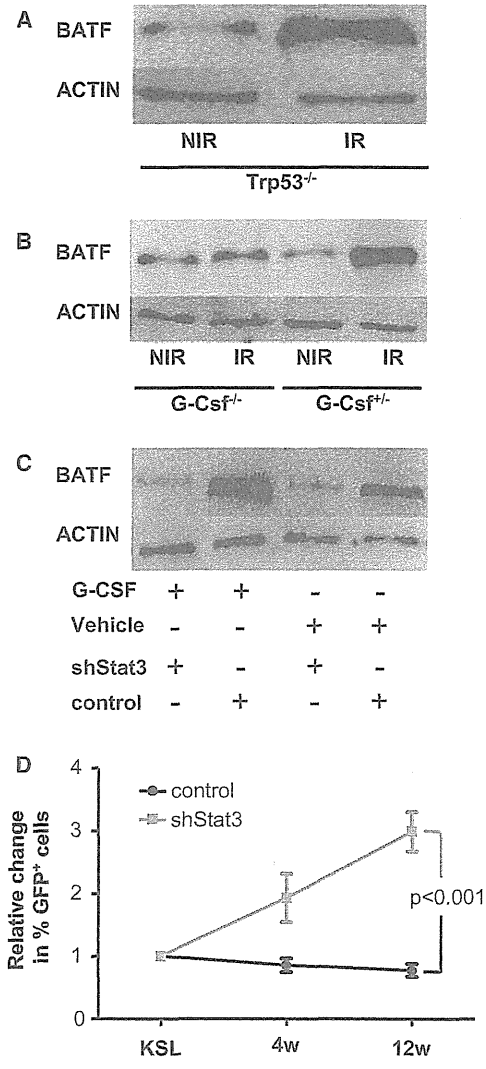

Figure 4. G-CSF/STAT3-Dependent Induction of BATF Limits the Repopulation Capacity of HSCs in Response to DNA Damage

(A–C) Representative Western blots showing the expression of BATF (A) in freshly isolated Lin$^-$ cells from irradiated (4 Gy, 6 hr after irradiation) and nonirradiated *Trp53*$^{-/-}$ mice (n = 2 mice per group), (B) in freshly isolated Lin$^-$ cells from irradiated (4 Gy, 6 hr after irradiation) and nonirradiated *G-Csf*$^{-/-}$ mice and *G-Csf*$^{+/-}$ mice (n = 3 mice per group), (C) in Lin$^-$ cells from donor mice that were transplanted with *Stat3* shRNA or a scrambled shRNA infected KSL cells (10 weeks after Tx). Freshly isolated, GFP positive, Lin$^-$ cells were purified and exposed for 3 days to G-CSF (10 ng/ml) or vehicle control (n = 2 repeat experiments).

(D) Freshly isolated KSL cells from *mTerc*$^{+/+}$ or G3 *mTerc*$^{-/-}$ mice (n = 3 donors per group) were infected with a *Stat3*-shRNA or a scrambled shRNA. The infection rate was 24%–35% and was normalized to 1. Infected cells were transplanted into lethally irradiated recipients along with noninfected cells from the same culture (n = 3 recipients for each group). The histogram depicts changes in peripheral blood chimerism of infected cells (GFP-positive) in primary recipients at the indicated time point after transplantation. Values are shown as mean ± SEM, n = 3 mice per group.

See Figure S4A.

BATF-Dependent Differentiation Leads to the Depletion of Myeloid and Lymphoid Competent HSCs in Response to Irradiation

The above data indicated that lymphoid competent (CD150^{lo}) HSCs were more sensitive to DNA damage-induced differentiation than myeloid competent HSCs (CD150^{hi}). However, an analysis of absolute HSC numbers at different time points after γ-irradiation revealed that the number of CD150^{hi} HSCs was also reduced within 24 hr after 4Gy γ-irradiation albeit less pronounced compared to CD150^{lo} HSCs (Figure 6A). At these early time points after γ-irradiation, there was only a slight induction of apoptosis (5%–10%) and proliferation rates remained almost unchanged in both CD150^{hi} and CD150^{lo} HSCs (Figures S6A and S6B) suggesting that other factors were involved in the observed changes in HSC numbers in response to IR. Previous studies on single cell transplantations suggested that CD150^{hi} HSCs can differentiate into CD150^{lo} HSCs (Morita et al., 2010). It was possible that this differentiation process was induced by DNA damage in response to IR. In agreement with this interpretation, we observed a transient increase in the number CD150^{lo} HSCs from 6 to 12 hr after γ-irradiation paralleling the reduction in the total number of CD150^{hi} HSCs (Figure 6A). Mathematical modeling revealed an improvement of model fitness for the observed kinetics of γ-irradiation-induced changes in HSC numbers when (1) differentiation of CD150^{hi} to CD150^{lo} HSCs and (2) depletion of CD150^{lo} HSCs by lymphoid differentiation were included into the equation (Figure 6B, Extended Experimental Procedures, Figures S6C–S6I). Plain models that were solely based on the rates of HSC proliferation (Figure S6A) and apoptosis (Figure S6B), exhibited significantly higher error values as they were fitted to the observed data (Figures 6C and 6D). To experimentally test this prediction, highly purified CD150^{hi} HSCs were transplanted into lethally irradiated recipient. 24 hr after transplantation, one half of the recipients were γ-irradiated (4 Gy), while the others remained nonirradiated (n = 4 mice per group). Analysis of donor-derived HSCs (24 hr after IR) confirmed that irradiation-induced the transition of CD150^{hi} into CD150^{lo} HSCs (Figure S6J). Mathematical modeling also supported the experimental data indicating that irradiation-induced lymphoid differentiation of 'true HSCs' within the populations of CD150^{hi} and CD150^{lo} HSCs (Figure 5, Extended Experimental Procedures, Figures S7A–S7E).

mRNA expression of *Batf* was significantly induced in freshly isolated HSCs of γ-irradiated mice (12 hr after IR) in both CD150^{hi} and CD150^{lo} HSCs (Figure S7F, n = 3 mice per group). To test the functional role of DNA damage-dependent BATF induction for the depletion of HSC subpopulations, γ-irradiation was applied (1) to *Batf*$^{-/-}$ and *Batf*$^{+/+}$ mice, (2) to mice that were long-term reconstituted with *Batf* shRNA or scrambled shRNA infected HSCs, and (3) to *G-Csf*$^{-/-}$ and *G-Csf*$^{+/-}$ mice. The depletion of CD150^{lo} HSCs and CD150^{hi} HSCs was significantly rescued in all 3 scenarios, while *Batf* or *G-Csf* gene status did not affect the number of CD150^{lo} or CD150^{hi} HSCs in nonirradiated recipients (Figures 6E–6G).

BATF Induction Contributes to Activation of DNA Damage Signals in HSCs

Restrictions in self-renewal and induction of differentiation of stem cells are associated with an activation of p53 and cell cycle

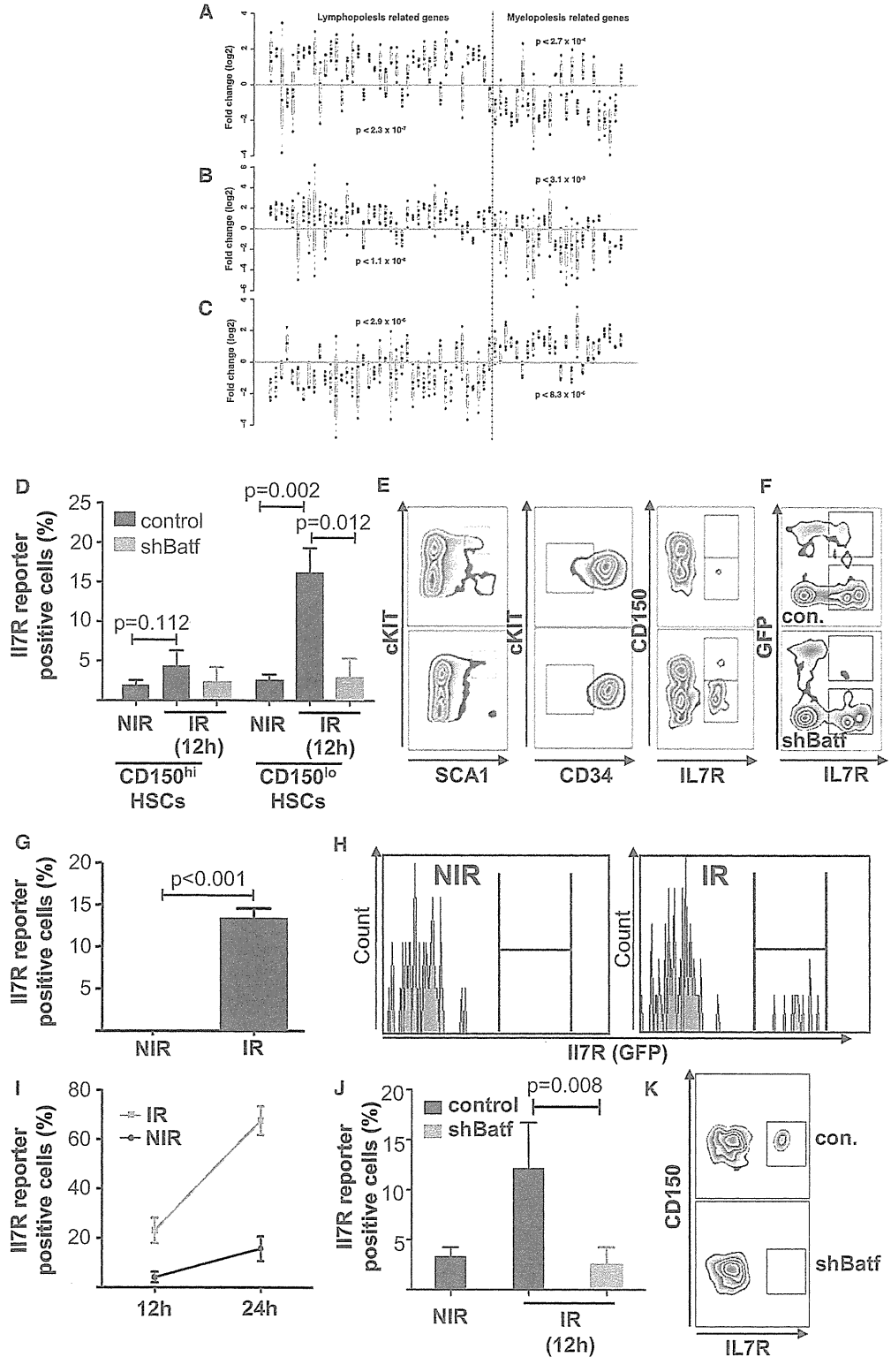
A
Lymphopoiesis related genes
Myelopoiesis related genes
p<2.7 x 10⁻⁴
p<2.3 x 10⁻⁷
Fold change (log2)
B
p<3.1 x 10⁻³
p<1.1 x 10⁻⁶
C
p<2.9 x 10⁻⁶
p<6.3 x 10⁻⁴
D
Il7R reporter positive cells (%)
control
shBatf
p=0.002
p=0.012
p=0.112
NIR
IR (12h)
CD150hi HSCs
CD150lo HSCs
E
cKIT
SCA1
CD34
CD150
IL7R
F
GFP
con.
shBatf
IL7R
G
p<0.001
H
NIR
IR
Count
Il7R (GFP)
I
IR
NIR
12h
24h
J
p=0.008
K
CD150

inhibitors (e.g., p21, p16) (Kastan et al., 1991, Topley et al., 1999, Akala et al., 2008, Choudhury et al., 2007). Here, p16 and p21 mRNA expression and p53 phosphorylation were analyzed in long-term engrafted mice (4 month) that were transplanted with *Batf*-shRNA versus scrambled-shRNA infected G3 *mTerc*$^{-/-}$ HSCs. This analysis revealed that the induction of p16, p21, and p53 phosphorylation in G3 *mTerc*$^{-/-}$ hematopoietic cells were *Batf*-dependent (Figures 7A–7D).

Activation of BATF in Human HSCs Correlates with Telomere Shortening and Activation of DNA Damage Signals

Myelodysplastic syndromes (MDS) are aging associated diseases of the hematopoietic system leading to bone marrow failure, skewed hematopoiesis, and a sharply increased risk of leukemia formation. MDS are characterized by increases in HSC proliferation and telomere shortening (Ohyashiki et al., 1994). Here, the expression of *Batf* and *p21* mRNA and telomere length were analyzed in freshly isolated CD34^{+} HSCs from bone marrow aspirates of MDS patients. Telomere shortening associated with increased *p21* mRNA expression indicating that telomere shortening led to an activation of DNA damage signals (Figure 7E). There was a direct association of BATF expression levels with p21 expression ($p = 0.005$) and an inverse association of BATF expression with telomere length ($p < 0.001$, Figures 7F and 7G). These data support the view that increases in BATF expression represent a conserved response to DNA damage in murine and human HSCs.

DISCUSSION

The current study provides experimental evidence for a differentiation checkpoint limiting self-renewal of HSCs in response to DNA damage. Melanocytic stem cells were previously shown to differentiate in response to γ-irradiation (Inomata et al., 2009). Our new data support the hypothesis that differentiation may represent a general response of tissue stem cells to DNA damage. The current study identified a molecular pathway controlling stem cell differentiation in response to DNA damage. Of note, this checkpoint depends on BATF - a transcription factor known to control lymphocyte differentiation in the hematopoietic system (Betz et al., 2010, Schraml et al., 2009). It is tempting to speculate that genotoxic stress enhances tissue specific differentiation pathways in stem cells as a default response to DNA damage.

Stem Cell Differentiation Checkpoints: Implication for Cancer Protection?

This study shows that abrogation of G-CSF/STAT3/BATF-dependent differentiation prolongs self-renewal of HSCs in the context of DNA damage but this rescue results in DNA damage accumulation in stem cells. These data indicate that differentiation represents an additional checkpoint layer to prevent survival of damaged stem cells possibly protecting from stem cell-derived cancers. The extreme quiescence of HSCs may have selected for this additional checkpoint. Recent studies showed that HSCs enter the cell cycle only once every 3–4 months (Wilson et al., 2008). It is conceivable that cell cycle arrest cannot prevent aberrant DNA repair, which is known to occur in quiescent HSCs (Mohrin et al., 2010). Since quiescent cells are also more resistant to DNA damage-induced cell death (Sullivan et al., 1987), it is possible that apoptosis can also fail to prevent the survival of quiescent HSCs harboring DNA damage. Together, the induction of differentiation may thus represent a critical failsafe mechanism eliminating quiescent stem cells that accumulate genotoxic damage.

Stem Cell Differentiation Checkpoints: Implication for Aging?

The *Batf* shRNA was most strongly selected in transplanted telomere dysfunctional HSCs compared to wild-type HSCs, also among other shRNAs in the iRNA library that targeted well known DNA damage checkpoint genes (Table S4). These data indicate that BATF represents a major pathway limiting HSC function in response to DNA damage. It is conceivable that this newly defined checkpoint affects aging of the hematopoietic system

Figure 5. DNA Damage Induces Lymphoid Differentiation of Hematopoietic Stem Cells

(A–C) The histograms show fold changes in the mRNA expression of lymphopoiesis and myelopoiesis-related genes (Table S3) in freshly isolated (A) HSCs (CD34^{-}KSL) from 8-10 month old G3 *mTerc*$^{-/-}$ versus *mTerc*$^{+/+}$ mice, (B) HSCs (CD34^{-}KSL) from 2 month old, nonirradiated versus irradiated *mTerc*$^{+/+}$ mice (4 Gy, 12 hr after IR), (C) GFP^{+} HSCs (CD34^{-}KSL) from recipient mice, 16 weeks after transplantation of shRNA-*Batf* versus scrambled shRNA targeted KSL cells from G3 *mTerc*$^{-/-}$ mice. Fold changes of the transcriptional signatures are shown as box blots in a log transformation so that a fold change of 1 is represented by a 0. The 2-sided Wilcoxon test was used to test the Null hypothesis of the fold change being equal to 1 (n = 2 pools of 4-6 mice per group).

(D–F) Mice were transplanted with total bone marrow from Il7R- reporter mice or with *Batf* shRNA transduced KSL cells from Il7R- reporter mice. Engrafted recipients were γ-irradiated with 4 Gy (IR) or remained nonirradiated (NIR) (n = 3-4 mice per group, values are shown as mean ± SD). 12 hr later, IL7R-reporter activity was analyzed in freshly isolated CD150^{hi} or CD150^{lo} HSCs. (D) The histogram shows the percentage of IL7R-reporter-positive cells in myeloid competent HSCs (CD150^{hi}) and in lymphoid competent HSCs (CD150^{lo}). (E) Representative FACS analysis of IL7R-reporter induction: gates in left panel indicate KSL cells, gates in middle panel indicate CD34^{-}KSL cells, gates in right panel show IL7R-reporter positive cells in CD150^{hi} (upper gates) and CD150^{lo} (lower gates) HSCs. (F) Representative FACS blots showing induction of IL7R-reporter activity in CD150^{lo} HSCs isolated from recipients that were transplanted with *Batf* shRNA or scrambled shRNA infected KSL cells from Il7R- reporter mice. Note that the induction of IL7R activity is impaired in *Batf* shRNA-infected HSCs (GFP^{+}, upper gate in lower panel) compared to scrambled shRNA infected HSCs (GFP^{+}, upper gate in upper panel). IR induces Il7R-reporter activity in noninfected HSCs in both cohorts (GFP-).

(G–I) Freshly isolated myeloid competent HSCs (CD150^{hi}CD34^{-}KSL cells) or lymphoid competent HSCs (CD150^{lo}CD34^{-}LSK cells) were seeded on OP9 feeder cells. The induction of IL7R-activity was measured in response to γ−irradiation (4Gy) and in nonirradiated controls (n = 3 repeat experiments, values are shown as mean ± SD), (G) The histogram shows the percentage of IL7R-positive cells in CD150^{hi}CD34^{-}KSL cells, 24 hr after IR versus non-IR, (H) representative FACS blots show the induction of IL7R-activity in CD150^{hi}CD34^{-}KSL cells, 24 hr after IR versus non-IR, (I) The histogram shows the percentage of IL7R-positive cells in CD150^{lo}CD34^{-}KSL cells, 12 and 24 hr after IR versus non-IR. Values are shown as mean ± SEM, n = 3 mice per group.

(J and K) CD150^{lo} HSCs were freshly isolated from recipients reconstituted with *Batf* shRNA or scrambled shRNA infected KSL cells from IL7R-reporter mice. 1500 freshly purified CD150^{lo} HSCs were sorted per well (n = 5 wells per group) and γ-irradiated with 4Gy (IR) or nonirradiated (NIR), followed by FACS analysis 12h later. (J) The histogram shows the induction of Il7R-reporter activity. Values are shown as mean ± SEM, n = 5 mice per group. (K) Representative FACS blots. See Figure S4, Figure S5, and Table S5.

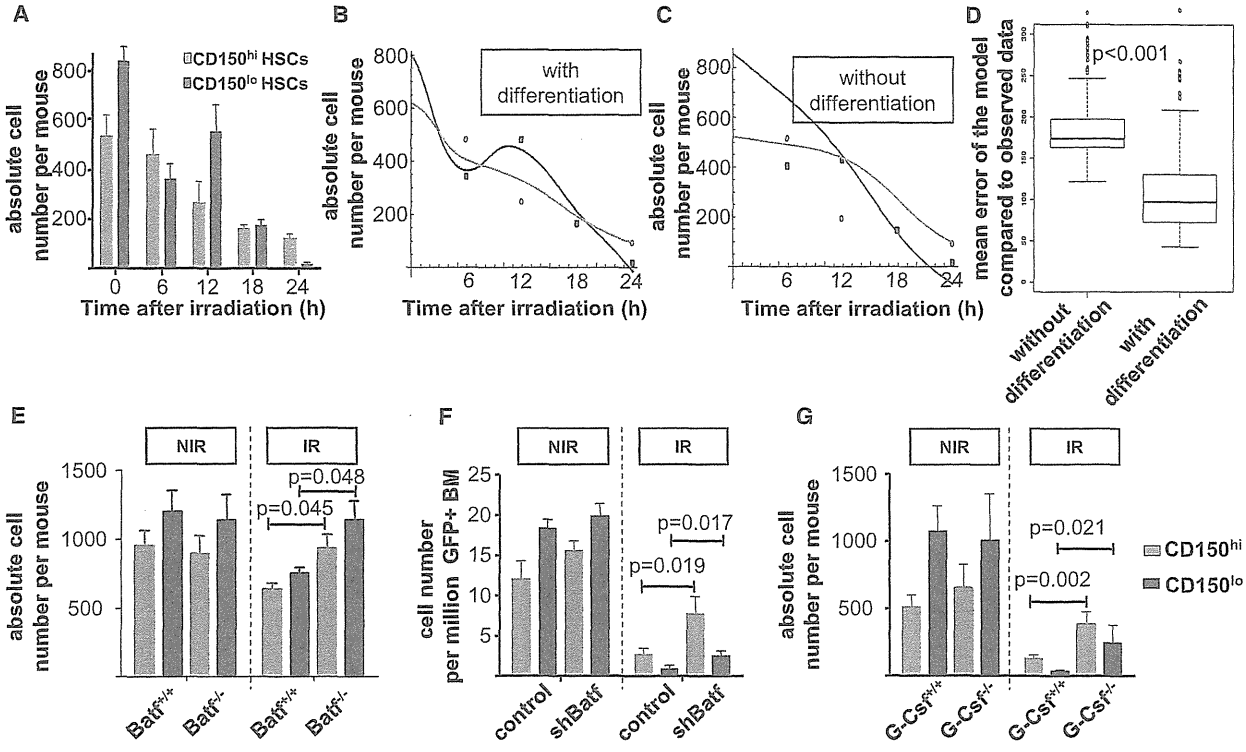

Figure 6. BATF-Dependent Differentiation Contributes to HSC Depletion in Response to γ-Irradiation

(A) Histogram showing the absolute number of CD150^{hi} and CD150^{lo} HSCs in bone marrow of 2 month old *mTerc*$^{+/+}$ mice at the indicated time points after 4 Gy γ-irradiation. Values are shown as mean ± SD, n = 3 mice per group for each time point.

(B–D) Mathematical modeling of the observed changes in cell number in response to irradiation: (C) Model without DNA damage-induced differentiation, solely based on changes of cell numbers by cell death and proliferation (Figure S6A,B), (B) DNA damage-induced differentiation was included in the delay-differential equations assuming that CD150^{hi} HSCs differentiated into CD150^{lo} HSCs and CD150^{lo} HSCs were depleted from the stem cell pool by induction of lymphocyte differentiation, (D) Box blot showing the mean error of cell numbers in mathematical models compared to the observed data.

(E–G) The histograms depict the number of CD150^{hi} and CD150^{lo} HSCs in: (E) irradiated (12 hr after IR) versus nonirradiated Batf$^{-/-}$ and Batf$^{+/+}$mice; (F) irradiated (24h after IR) versus nonirradiated recipients of *Batf* shRNA or scrambled shRNA (control) infected KSL cells (4 months after transplantation); (G) irradiated (24 hr after IR) versus nonirradiated *G-Csf*$^{-/-}$ and *G-Csf*$^{+/-}$ mice (n = 5 mice per group). (E–G) Values are shown as mean ± SEM, n = 4–5 mice per group.

See Extended Experimental Procedures and Figure S6 and Figure S7.

since there is growing evidence for DNA damage accumulation in aging HSCs (Rossi et al., 2007, Rübe et al., 2011).

Impaired replication potential and skewing in differentiation represent the most prominent phenotypes of the aging hematpoietic system. Studies on the cellular composition of bone marrow-derived HSCs in mice revealed evidence that the HSC pool consists of distinct subpopulations exhibiting a different potential to undergo myeloid or lymphoid differentiation (Challen et al., 2010). Aging associated skewing of hematopoiesis was recently associated with an increased survival of myeloid competent HSCs in aging mice supporting a population shift model of HSC aging (Cho et al., 2008, Beerman et al., 2010). According to this model myeloid competent HSCs are selected and outcompete lymphoid competent HSCs during aging. The molecular mechanisms that control this selection process during aging are unknown. The current study shows that BATF-dependent differentiation limits the repopulation capacity and self-renewal of HSCs in response to telomere dysfunction or γ-irradiation. Since lymphoid competent HSCs (CD150^{lo}) were more sensitive to this checkpoint, it is possible that BATF upregulation contributes to the ablation of lymphoid competent HSCs in response to aging associated DNA damage accumulation.

In summary, the current study provides evidence for a G-CSF/Stat3/BATF-dependent checkpoint, which limits self-renewal of HSCs in response to DNA damage or telomere dysfunction by induction of lymphoid differentiation. These data support a new concept indicating that DNA damage limits self-renewal of damaged stem cells by activating tissue specific differentiation pathways. The newly discovered differentiation checkpoint appears to be conserved in human HSCs and could impact on age-associated changes in stem cell differentiation and transformation in the hematopoietic system.

EXPERIMENTAL PROCEDURES

Mice

Mice were maintained in a pathogen-free environment and fed with a standard diet. All mice were in a C57BL6J background. Animal experiments were

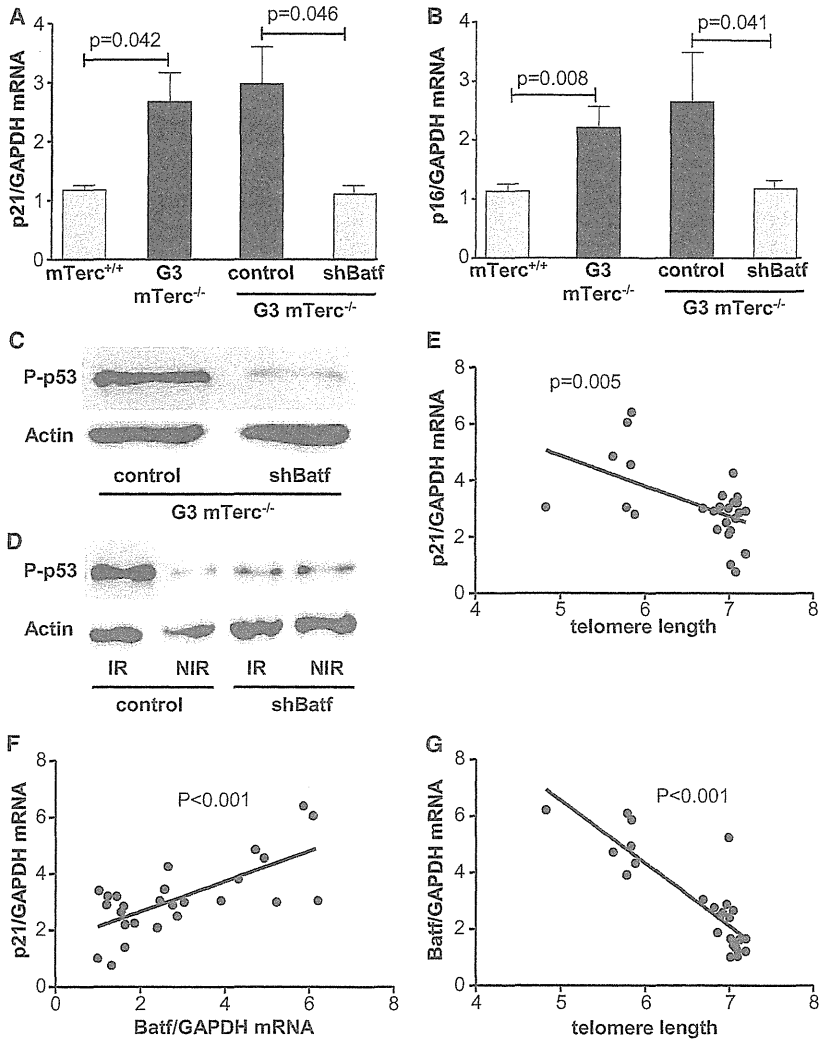

Figure 7. DNA Damage-Dependent Upregulation of BATF in Hematopoietic Cells Contributes to the Activation of Checkpoint Genes and Is Maintained in Human CD34$^+$ Hematopoietic Cells

(A and B) Histograms showing mRNA expression of p21 (A) and p16 (B) relative to GAPDH in freshly isolated HSCs (CD34$^-$KSL) from 8-10 month old *mTerc*$^{+/+}$ and G3 *mTerc*$^{-/-}$ mice, and from long-term reconstituted mice, 16 weeks after transplantation of hematopoietic cells from G3 *mTerc*$^{-/-}$ that were transduced with a *Batf* shRNA or a scrambled shRNA (n = 3 per group, values are shown as mean ± SEM).

(C) Representative Western blot showing the expression of phospho-p53 in freshly isolated Lin$^-$ cells from bone marrow of long-term reconstituted mice, 16 weeks after transplantation of shRNA-*Batf* or scrambled shRNA transduced G3 *mTerc*$^{-/-}$ hematopoietic cells (n = 3 mice per group).

(D) Hematopoietic cells from *mTerc*$^{+/+}$ mice were transduced with shRNA-*Batf* or scrambled shRNA and transplanted into lethally irradiated recipients. Two months after transplantation one group of the recipients was irradiated with 4 Gy γ-irradiation. Representative Western blot showing the expression of phospho-p53 in freshly isolated Lin$^-$ cells from bone marrow of nonirradiated and irradiated recipients (6 hr after IR, n = 3 mice per group). Note that shRNA knockdown of *Batf* impaired γ-irradiation induced p53 phosphorylation.

(E–G) Telomere length and the mRNA expression of p16 and *Batf* (relative to *Gapdh*) was measured in CD34$^+$ human HSCs from patients with myelodysplastic syndrome (MDS, n = 26): The histograms show (E) the correlation between p21 mRNA level and telomere length, (F) p21 mRNA level and *Batf* mRNA level, and (G) Batf mRNA level and telomere length. Note that telomere shortening and the induction of p21 correlates with induction of *Batf* in human CD34$^+$ HSCs.

approved by the state government of Baden-Württemberg (Protocol Number 35/9185.81-3/919).

Plasmid and Lentiviral Vector Construction

SF-LV-shRNA-EGFP: the spleen-focus forming promoter (SFFV) driven GFP expression cassette was inserted into the lentiviral GIPZ (Open Biosystems, Huntsville, USA) vector. The IRES-puromycin cassette was replaced by the 120bp fragment harboring the 5′mir30 sequence: 5′mir30 5′-AGCGGCCG CAAATTCCGGTTTGTTTGAATGAGGCTTCAGTACTT-3′ and 3′mir30 5′-TAC CTCGACTCGAGCCTTCTGTT-3′ to create the final vector SF-LV-shRNA-EGFP.

Lentivirus Production

Lentivirus was produced in 293T cells after transfection of 20μg shRNA plasmid, 15 μg pCMVΔR8.91 helper plasmid and 6 μg pMD.G according to standard procedures (Schambach et al., 2006). Virus was concentrated by centrifugation at 25,000rpm for 2.5 hr, 4°C, virus pellet was resuspended in sterile PBS.

cDNA Clone

Batf cDNA was amplified (forward primer: ACTGCTCGAGGCCACCATGCCT CACAGCTCCG and reverse primer: CAGTGCGGCCGCAACTATCCACCCC CTGC) and inserted into SF-LV-cDNA-EGFP.

Western Blot

Whole-cell extracts were obtained in RIPA buffer and subjected to 15% SDS-PAGE using antibodies against BATF (1:1000, Abnova and Abcam), phosphor-p53-Ser15 (1:1000, Cell Signaling) and beta-actin (1:10000, Sigma).

For HSC analysis bone marrow was collected from five 12 month old mice. Lin$^-$cells were purified by MACS, followed by FACS purification of 3x10^4 CD34$^-$KSL cells. Cells were lysed in loading buffer (50mM Tris base pH6.8, 4% SDS, 0.04% Bromphenolblau, 20% glycerol) and the entire lysate was loaded after boiling.

shRNA Recovery

Genomic DNA was isolated from lineage negative bone marrow cells (Gentra Puregene Blood Kit, QIAGEN) and the integrated proviral sequences were amplified with primers flanking the mir30 cassette (for details see Zuber et al., 2011).

RNA Isolation

Total RNA was isolated from freshly isolated and sorted HSCs by using MagMAX 96 total RNA isolation Kit (Ambion) due to the manufactors protocol.

Quantitative Real-Time PCR

Quantitative real-time PCR was performed with an ABI 7300 Real-Time PCR System (Applied Biosystems) in duplicates from at least 3 biological samples. The superscript III kit (Invitrogen) was used for cDNA synthesis from total RNA. Table S4 depicts primer sets for the detection of single genes. The quantitative PCR was carried out in a volume of 25μl using the iTaq SYBR Green supermix with Rox (Bio-Rad).

Flow Cytometry

For flow cytometric analysis, and sorting, hind limb bones were dissected and single-cell suspensions were stained with antibodies, as previously described (Ema et al., 2006). Data acquisition and cell sorting were performed on FACS LSRII and FACSAriaII (BD Biosciences). Data were analyzed with the FlowJo software.

Statistics

SPSS 11.5 was used for statistical analyses. Unpaired Student's t test and Chi-Square Test was used to generate *P* values for most of the datasets. Otherwise it is stated in the figure legends.

Mathematical Modeling

Delay-differential equations were used to model changes in cell numbers and integrated numerically (Mathematica V8, Wolfram Research). Functions for effects of proliferation and apoptosis were fitted to data from the experiments (see Supplemental Experimental Methods, Figure 6A, Figure S6). Differentiation was modeled as occurring within a specific time frame (100 runs with random starting values, latin hypercube sampling). Measured cell numbers were utilized resulting in $3^5 = 243$ possible combinations of data points. We fitted models including differentiation and simplified models without differentiation to each combination (comparison via the Wilcoxon test).

SUPPLEMENTAL INFORMATION

Supplemental Information includes Extended Experimental Procedures, five tables, and seven figures and can be found with this article online at doi:10.1016/j.cell.2012.01.040.

ACKNOWLEDGMENTS

This work was supported by the DFG (Ru745-11 and −10, by the SFB497/C11, ZE545-2), the European Union (Telomarker), the BMBF (SyStaR), and by the International Graduate School in Molecular Medicine at Ulm University (GSC270). We thank Susan Schlenner and Hans-Reimer Rodewald for providing *IL7R* Cre reporter mice and Hans-Joerg Fehling for providing *ROSA RFP* mice.

Received: April 7, 2011
Revised: September 22, 2011
Accepted: January 25, 2012
Published: March 1, 2012

REFERENCES

Akala, O.O., Park, I.K., Qian, D., Pihalja, M., Becker, M.W., and Clarke, M.F. (2008). Long-term haematopoietic reconstitution by Trp53−/−p16Ink4a−/− p19Arf−/− multipotent progenitors. Nature *453*, 228–232.

Allsopp, R.C., Morin, G.B., DePinho, R.A., Harley, C.B., and Weissman, I.L. (2003). Telomerase is required to slow telomere shortening and extend replicative lifespan of HSCs during serial transplantation. Blood *102*, 517–520.

Beausejour, C.M., and Campisi, J. (2006). Ageing: balancing regeneration and cancer. Nature *443*, 404–405.

Beerman, I., Bhattacharya, D., Zandi, S., Sigvardsson, M., Weissman, I.L., Bryder, D., and Rossi, D.J. (2010). Functionally distinct hematopoietic stem cells modulate hematopoietic lineage potential during aging by a mechanism of clonal expansion. Proc. Natl. Acad. Sci. USA *107*, 5465–5470.

Betz, B.C., Jordan-Williams, K.L., Wang, C., Kang, S.G., Liao, J., Logan, M.R., Kim, C.H., and Taparowsky, E.J. (2010). Batf coordinates multiple aspects of B and T cell function required for normal antibody responses. J. Exp. Med. *207*, 933–942.

Bric, A., Miething, C., Bialucha, C.U., Scuoppo, C., Zender, L., Krasnitz, A., Xuan, Z., Zuber, J., Wigler, M., Hicks, J., et al. (2009). Functional identification of tumor-suppressor genes through an in vivo RNA interference screen in a mouse lymphoma model. Cancer Cell *16*, 324–335.

Challen, G.A., Boles, N.C., Chambers, S.M., and Goodell, M.A. (2010). Distinct hematopoietic stem cell subtypes are differentially regulated by TGF-beta1. Cell Stem Cell *6*, 265–278.

Chin, L., Artandi, S.E., Shen, Q., Tam, A., Lee, S.L., Gottlieb, G.J., Greider, C.W., and DePinho, R.A. (1999). p53 deficiency rescues the adverse effects of telomere loss and cooperates with telomere dysfunction to accelerate carcinogenesis. Cell *97*, 527–538.

Cho, R.H., Sieburg, H.B., and Muller-Sieburg, C.E. (2008). A new mechanism for the aging of hematopoietic stem cells: aging changes the clonal composition of the stem cell compartment but not individual stem cells. Blood *111*, 5553–5561.

Choudhury, A.R., Ju, Z., Djojosubroto, M.W., Schienke, A., Lechel, A., Schaetzlein, S., Jiang, H., Stepczynska, A., Wang, C., Buer, J., et al. (2007). Cdkn1a deletion improves stem cell function and lifespan of mice with dysfunctional telomeres without accelerating cancer formation. Nat. Genet. *39*, 99–105.

d'Adda di Fagagna, F., Reaper, P.M., Clay-Farrace, L., Fiegler, H., Carr, P., von Zglinicki, T., Saretzki, G., Carter, N.P., and Jackson, S.P. (2003). A DNA damage checkpoint response in telomere-initiated senescence. Nature *426*, 194–198.

Dorsey, M.J., Tae, H.J., Sollenberger, K.G., Mascarenhas, N.T., Johansen, L.M., and Taparowsky, E.J. (1995). B-ATF: a novel human bZIP protein that associates with members of the AP-1 transcription factor family. Oncogene *11*, 2255–2265.

Ema, H., Morita, Y., Yamazaki, S., Matsubara, A., Seita, J., Tadokoro, Y., Kondo, H., Takano, H., and Nakauchi, H. (2006). Adult mouse hematopoietic stem cells: purification and single-cell assays. Nat. Protoc. *1*, 2979–2987.

Hoeijmakers, J.H. (2009). DNA damage, aging, and cancer. N. Engl. J. Med. *361*, 1475–1485.

Hope, K.J., Cellot, S., Ting, S.B., MacRae, T., Mayotte, N., Iscove, N.N., and Sauvageau, G. (2010). An RNAi screen identifies Msi2 and Prox1 as having opposite roles in the regulation of hematopoietic stem cell activity. Cell Stem Cell *7*, 101–113.

Inomata, K., Aoto, T., Binh, N.T., Okamoto, N., Tanimura, S., Wakayama, T., Iseki, S., Hara, E., Masunaga, T., Shimizu, H., et al. (2009). Genotoxic stress abrogates renewal of melanocyte stem cells by triggering their differentiation. Cell *137*, 1088–1099.

Janzen, V., Forkert, R., Fleming, H.E., Saito, Y., Waring, M.T., Dombkowski, D.M., Cheng, T., DePinho, R.A., Sharpless, N.E., and Scadden, D.T. (2006). Stem-cell ageing modified by the cyclin-dependent kinase inhibitor p16INK4a. Nature *443*, 421–426.

Kastan, M.B., Radin, A.I., Kuerbitz, S.J., Onyekwere, O., Wolkow, C.A., Civin, C.I., Stone, K.D., Woo, T., Ravindranath, Y., and Craig, R.W. (1991). Levels of p53 protein increase with maturation in human hematopoietic cells. Cancer Res. *51*, 4279–4286.

Kiel, M.J., Yilmaz, O.H., Iwashita, T., Terhorst, C., and Morrison, S.J. (2005). SLAM family receptors distinguish hematopoietic stem and progenitor cells and reveal endothelial niches for stem cells. Cell *121*, 1109–1121.

Kiel, M.J., Yilmaz, O.H., and Morrison, S.J. (2008). CD150- cells are transiently reconstituting multipotent progenitors with little or no stem cell activity. Blood *111*, 4413–4414.

Lee, H.W., Blasco, M.A., Gottlieb, G.J., Horner, J.W., Greider, C.W., and DePinho, R.A. (1998). Essential role of mouse telomerase in highly proliferative organs. Nature *392*, 569–574.

Linton, P.J., and Dorshkind, K. (2004). Age-related changes in lymphocyte development and function. Nat. Immunol. *5*, 133–139.

Liu, Y., Johnson, S.M., Fedoriw, Y., Rogers, A.B., Yuan, H., Krishnamurthy, J., and Sharpless, N.E. (2011). Expression of p16INK4a prevents cancer and promotes aging in lymphocytes. Blood *117*, 3257–3267.

Mohrin, M., Bourke, E., Alexander, D., Warr, M.R., Barry-Holson, K., Le Beau, M.M., Morrison, C.G., and Passegué, E. (2010). Hematopoietic stem cell quiescence promotes error-prone DNA repair and mutagenesis. Cell Stem Cell *7*, 174–185.

Molofsky, A.V., Slutsky, S.G., Joseph, N.M., He, S., Pardal, R., Krishnamurthy, J., Sharpless, N.E., and Morrison, S.J. (2006). Increasing p16INK4a expression decreases forebrain progenitors and neurogenesis during ageing. Nature *443*, 448–452.

Morita, Y., Ema, H., and Nakauchi, H. (2010). Heterogeneity and hierarchy within the most primitive hematopoietic stem cell compartment. J. Exp. Med. *207*, 1173–1182.

Morrison, S.J., Wandycz, A.M., Akashi, K., Globerson, A., and Weissman, I.L. (1996). The aging of hematopoietic stem cells. Nat. Med. *2*, 1011–1016.

Nishino, J., Kim, I., Chada, K., and Morrison, S.J. (2008). Hmga2 promotes neural stem cell self-renewal in young but not old mice by reducing p16Ink4a and p19Arf Expression. Cell *135*, 227–239.

Ohyashiki, J.H., Ohyashiki, K., Fujimura, T., Kawakubo, K., Shimamoto, T., Iwabuchi, A., and Toyama, K. (1994). Telomere shortening associated with disease evolution patterns in myelodysplastic syndromes. Cancer Res. *54*, 3557–3560.

Pelicci, P.G. (2004). Do tumor-suppressive mechanisms contribute to organism aging by inducing stem cell senescence? J. Clin. Invest. *113*, 4–7.

Rando, T.A. (2006). Stem cells, ageing and the quest for immortality. Nature *441*, 1080–1086.

Rossi, D.J., Bryder, D., Zahn, J.M., Ahlenius, H., Sonu, R., Wagers, A.J., and Weissman, I.L. (2005). Cell intrinsic alterations underlie hematopoietic stem cell aging. Proc. Natl. Acad. Sci. USA *102*, 9194–9199.

Rossi, D.J., Bryder, D., Seita, J., Nussenzweig, A., Hoeijmakers, J., and Weissman, I.L. (2007). Deficiencies in DNA damage repair limit the function of haematopoietic stem cells with age. Nature *447*, 725–729.

Rossi, D.J., Jamieson, C.H., and Weissman, I.L. (2008). Stems cells and the pathways to aging and cancer. Cell *132*, 681–696.

Rübe, C.E., Fricke, A., Widmann, T.A., Fürst, T., Madry, H., Pfreundschuh, M., and Rübe, C. (2011). Accumulation of DNA Damage in Hematopoietic Stem and Progenitor Cells during Human Aging. PLoS ONE *6*, e17487.

Rudolph, K.L., Chang, S., Lee, H.W., Blasco, M., Gottlieb, G.J., Greider, C., and Depinho, R.A. (1999). Longevity, stress response, and cancer in aging telomerase-deficient mice. Cell *96*, 701–712.

Sahin, E., and DePinho, R.A. (2010). Linking functional decline of telomeres, mitochondria and stem cells during ageing. Nature *464*, 520–528.

Schaetzlein, S., Kodandaramireddy, N.R., Ju, Z., Lechel, A., Stepczynska, A., Lilli, D.R., Clark, A.B., Rudolph, C., Kuhnel, F., Wei, K., et al. (2007). Exonuclease-1 deletion impairs DNA damage signaling and prolongs lifespan of telomere-dysfunctional mice. Cell *130*, 863–877.

Schambach, A., Galla, M., Modlich, U., Will, E., Chandra, S., Reeves, L., Colbert, M., Williams, D.A., von Kalle, C., and Baum, C. (2006). Lentiviral vectors pseudotyped with murine ecotropic envelope: increased biosafety and convenience in preclinical research. Exp. Hematol. *34*, 588–592.

Schlenner, S.M., Madan, V., Busch, K., Tietz, A., Läufle, C., Costa, C., Blum, C., Fehling, H.J., and Rodewald, H.R. (2010). Fate mapping reveals separate origins of T cells and myeloid lineages in the thymus. Immunity *32*, 426–436.

Schraml, B.U., Hildner, K., Ise, W., Lee, W.L., Smith, W.A., Solomon, B., Sahota, G., Sim, J., Mukasa, R., Cemerski, S., et al. (2009). The AP-1 transcription factor Batf controls T(H)17 differentiation. Nature *460*, 405–409.

Senga, T., Iwamoto, T., Humphrey, S.E., Yokota, T., Taparowsky, E.J., and Hamaguchi, M. (2002). Stat3-dependent induction of BATF in M1 mouse myeloid leukemia cells. Oncogene *21*, 8186–8191.

Sharpless, N.E., and DePinho, R.A. (2007). How stem cells age and why this makes us grow old. Nat. Rev. Mol. Cell Biol. *8*, 703–713.

Signer, R.A., Montecino-Rodriguez, E., Witte, O.N., and Dorshkind, K. (2008). Aging and cancer resistance in lymphoid progenitors are linked processes conferred by p16Ink4a and Arf. Genes Dev. *22*, 3115–3120.

Sudo, K., Ema, H., Morita, Y., and Nakauchi, H. (2000). Age-associated characteristics of murine hematopoietic stem cells. J. Exp. Med. *192*, 1273–1280.

Sullivan, D.M., Latham, M.D., and Ross, W.E. (1987). Proliferation-dependent topoisomerase II content as a determinant of antineoplastic drug action in human, mouse, and Chinese hamster ovary cells. Cancer Res. *47*, 3973–3979.

Tian, S.S., Lamb, P., Seidel, H.M., Stein, R.B., and Rosen, J. (1994). Rapid activation of the STAT3 transcription factor by granulocyte colony-stimulating factor. Blood *84*, 1760–1764.

Topley, G.I., Okuyama, R., Gonzales, J.G., Conti, C., and Dotto, G.P. (1999). p21(WAF1/Cip1) functions as a suppressor of malignant skin tumor formation and a determinant of keratinocyte stem-cell potential. Proc. Natl. Acad. Sci. USA *96*, 9089–9094.

Wang, J., Geiger, H., and Rudolph, K.L. (2011). Immunoaging induced by hematopoietic stem cell aging. Curr. Opin. Immunol. *23*, 532–536.

Wilson, A., Laurenti, E., Oser, G., van der Wath, R.C., Blanco-Bose, W., Jaworski, M., Offner, S., Dunant, C.F., Eshkind, L., Bockamp, E., et al. (2008). Hematopoietic stem cells reversibly switch from dormancy to self-renewal during homeostasis and repair. Cell *135*, 1118–1129.

Wong, K.K., Maser, R.S., Bachoo, R.M., Menon, J., Carrasco, D.R., Gu, Y., Alt, F.W., and DePinho, R.A. (2003). Telomere dysfunction and Atm deficiency compromises organ homeostasis and accelerates ageing. Nature *421*, 643–648.

Wright, W.E., and Shay, J.W. (1992). Telomere positional effects and the regulation of cellular senescence. Trends Genet. *8*, 193–197.

Zender, L., Xue, W., Zuber, J., Semighini, C.P., Krasnitz, A., Ma, B., Zender, P., Kubicka, S., Luk, J.M., Schirmacher, P., et al. (2008). An oncogenomics-based in vivo RNAi screen identifies tumor suppressors in liver cancer. Cell *135*, 852–864.

Zuber, J., Shi, J., Wang, E., Rappaport, A.R., Herrmann, H., Sison, E.A., Magoon, D., Qi, J., Blatt, K., Wunderlich, M., Taylor, M.J., and Vakoc, C.R. (2011). Nature *478*, 524–528.

Published February 20, 2012

JEM

Brief Definitive Report

Lethal myelofibrosis induced by *Bmi1*-deficient hematopoietic cells unveils a tumor suppressor function of the polycomb group genes

Hideyuki Oguro,[1,6] Jin Yuan,[1,6] Satomi Tanaka,[1,2] Satoru Miyagi,[1,6] Makiko Mochizuki-Kashio,[1,6] Hitoshi Ichikawa,[3] Satoshi Yamazaki,[4,7] Haruhiko Koseki,[5] Hiromitsu Nakauchi,[4,7] and Atsushi Iwama[1,6]

[1]Department of Cellular and Molecular Medicine, Graduate School of Medicine, Chiba University, Chiba 260-8670, Japan
[2]Department of Hematology, Chiba University Hospital, Chiba 260-8670, Japan
[3]Division of Genetics, National Cancer Center Research Institute, Tokyo 104-0045, Japan
[4]Division of Stem Cell Therapy, Center for Stem Cell Biology and Regenerative Medicine, Institute of Medical Science, University of Tokyo, Tokyo 108-8639, Japan
[5]Laboratory for Lymphocyte Development, RIKEN Research Center for Allergy and Immunology, Yokohama 230-0045, Japan
[6]Japan Science and Technology Agency (JST), Core Research for Evolutional Science and Technology and [7]ERATO, Gobancho, Chiyoda-ku, Tokyo 102-0076, Japan

Polycomb-group (PcG) proteins form the multiprotein polycomb repressive complexes (PRC) 1 and 2, and function as transcriptional repressors through histone modifications. They maintain the proliferative capacity of hematopoietic stem and progenitor cells by repressing the transcription of tumor suppressor genes, namely *Ink4a* and *Arf*, and thus have been characterized as oncogenes. However, the identification of inactivating mutations in the PcG gene, *EZH2*, unveiled a tumor suppressor function in myeloid malignancies, including primary myelofibrosis (PMF). Here, we show that loss of another PcG gene, *Bmi1*, causes pathological hematopoiesis similar to PMF. In a mouse model, loss of *Bmi1* in *Ink4a-Arf*$^{-/-}$ hematopoietic cells induced abnormal megakaryocytopoiesis accompanied by marked extramedullary hematopoiesis, which eventually resulted in lethal myelofibrosis. Absence of Bmi1 caused derepression of a cohort of genes, including *Hmga2*, which is an oncogene overexpressed in PMF. Chromatin immunoprecipitation assays revealed that Bmi1 directly represses the transcription of *Hmga2*. Overexpression of *Hmga2* in hematopoietic stem cells induced a myeloproliferative state with enhanced megakaryocytopoiesis in mice, implicating *Hmga2* in the development of pathological hematopoiesis in the absence of Bmi1. Our findings provide the first genetic evidence of a tumor suppressor function of Bmi1 and uncover the role of PcG proteins in restricting growth by silencing oncogenes.

CORRESPONDENCE
Atsushi Iwama:
aiwama@faculty.chiba-u.jp

Abbreviations used: CFC, colony-forming cell; ChIP, chromatin immunoprecipitation; CLP, common lymphoid progenitor; CMP, common myeloid progenitor; GMP, granulocyte/macrophage progenitor; H2Aub1, monoubiquitination of histone H2A; HPP-CFC, high proliferative potential-CFC; HSC, hematopoietic stem cell; LMPP, lymphoid-primed MPP; LSC, leukemic stem cell; LSK, Lineage$^-$Sca-1$^+$c-Kit$^+$; MEP, megakaryocyte/erythroid progenitor; MPN, myeloproliferative neoplasm; MPP, multipotent progenitor; PcG, polycomb-group; PMF, primary myelofibrosis; PRC, polycomb repressive complex.

Polycomb-group (PcG) proteins are transcriptional repressors that function in gene silencing by modulating chromatin structure. They form the chromatin-associated multiprotein complexes, polycomb repressive complex (PRC) 1 and PRC2 (Simon and Kingston, 2009). PcG proteins have been implicated in the maintenance of self-renewing stem cells (Pietersen and van Lohuizen, 2008; Konuma et al., 2010; Sauvageau and Sauvageau, 2010). Among *PcG* genes, *Bmi1* plays a central role in the inheritance of the stemness of somatic stem cells, including hematopoietic stem cells (HSCs) and neural stem cells (Park et al., 2003; Iwama et al., 2004; Molofsky et al., 2003), and its forced expression augments their self-renewal capability (Iwama et al., 2004). One of the major targets of Bmi1 is the *Ink4a/Arf* tumor suppressor gene locus, and deletion of both *Ink4a* and *Arf* in *Bmi1*-deficient mice substantially restores the defective self-renewal capacity of HSCs (Oguro et al., 2006). PcG and trithorax-group proteins mark developmental regulator gene promoters with bivalent domains consisting of overlapping repressive and activating

H. Oguro and J. Yuan contributed equally to this paper.

The Rockefeller University Press $30.00
J. Exp. Med. Vol. 209 No. 3 445-454
www.jem.org/cgi/doi/10.1084/jem.20111709

Published February 20, 2012

histone modifications to keep them poised for activation in embryonic stem cells (Pietersen and van Lohuizen, 2008; Konuma et al., 2010). Likewise, we found that Bmi1 reinforces bivalent histone domains at key hematopoietic regulator gene promoters in multipotent hematopoietic stem and progenitor cells to maintain their multipotency (Oguro et al., 2010). Thus, Bmi1 functions in the maintenance of both the self-renewal capacity and multipotency of HSCs.

Bmi1 has also been implicated in the maintenance of the proliferative capacity of leukemic stem cells (LSCs). Co-expression of *HoxA9* and *Meis1*, which can transform HSCs, induces leukemia from *Bmi1*-deficient fetal liver cells in primary recipient mice, but fails to sustain a leukemic state in the secondary recipients (Lessard and Sauvageau, 2003), suggesting that Bmi1 regulates the self-renewal of both HSCs and LSCs. In addition, we have recently reported that Bmi1 is essential for the faithful reprogramming of myeloid progenitors into LSCs, and that leukemic fusion genes require PcG proteins acting in concert to establish LSC-specific transcriptional profiles that confer full leukemogenic activity on LSCs (Yuan et al., 2011). Notably, a gain-of-function mutation of the PRC2 gene, *EZH2*, has recently been identified in a subset of lymphoma (Morin et al., 2010), highlighting the oncogenic properties of PRC2 genes. In contrast, inactivating mutations of *EZH2* have also been identified in patients with myelodysplastic syndrome and myeloproliferative neoplasms (MPN), revealing that *EZH2* also has a tumor suppressor function (Ernst et al., 2010; Nikoloski et al., 2010).

In this study, we found that *Bmi1* antagonizes development of MPN in the absence of its major tumor-suppressive targets, *Ink4a* and *Arf*, and identified *Hmga2*, an oncogene, as one of the direct targets of Bmi1 involved in the development of MPN. Our findings suggest that PcG genes fine-tune the hematopoietic homeostasis by balancing the transcription of oncogenic and tumor suppressive target genes.

RESULTS AND DISCUSSION

Loss of Bmi1 augments repopulating capacity of BM cells in an *Ink4a/Arf*-null background

We previously reported that deletion of both *Ink4a* and *Arf* in *Bmi1*-deficient mice substantially restores the defective self-renewal capacity of HSCs (Oguro et al., 2006). In this study, we performed competitive repopulation assays using the same number of BM competitor cells as the test cells, and found that *Bmi1*$^{-/-}$*Ink4a-Arf*$^{-/-}$ cells had higher repopulating activity in recipient mice than the wild-type and *Ink4a-Arf*$^{-/-}$

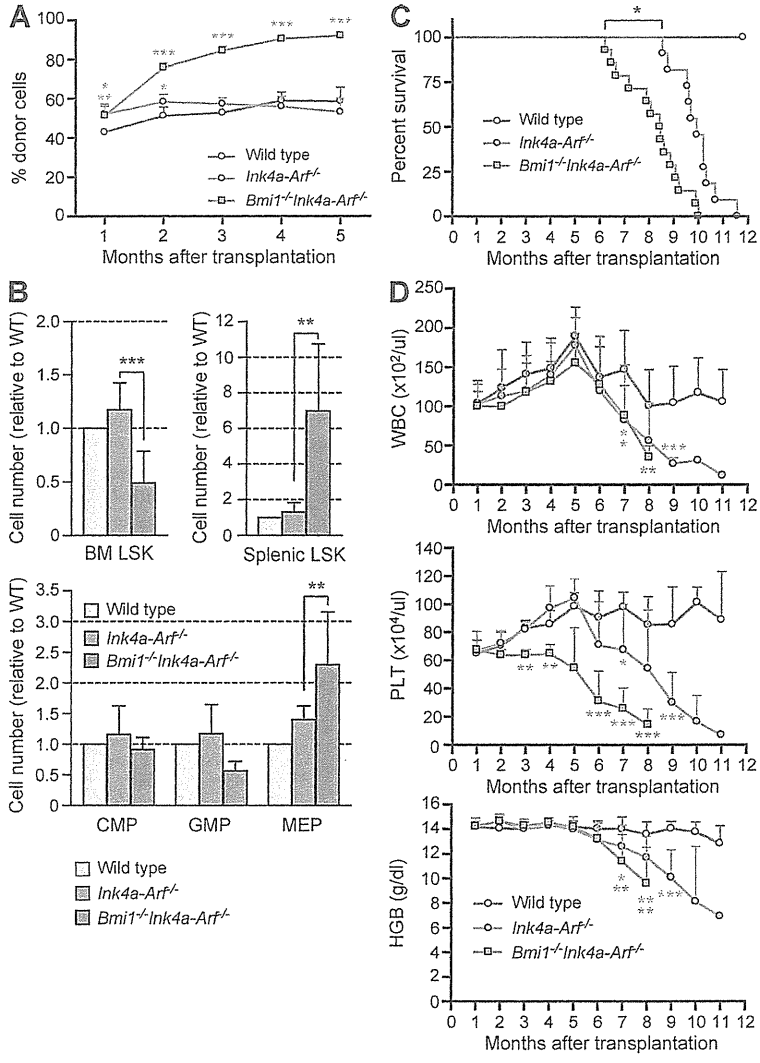

Figure 1. Loss of *Bmi1* augments the repopulating capacity of BM cells in the absence of *Ink4a/Arf*. (A) To perform a competitive repopulating assay, 10^6 pooled test BM cells from 4-wk-old mice (CD45.2$^+$) of the indicated genotype were mixed with 10^6 competitor BM cells (CD45.1$^+$) and injected into lethally irradiated recipient mice (CD45.1$^+$). The percent chimerism of donor cells in the recipient PB is presented as the mean ± SD (n = 5). *, P < 0.05; **, P < 0.01; ***, P < 0.001. (B) Relative numbers of donor-derived BM and splenic LSK cells, and BM CMPs, GMPs, and MEPs. Lethally irradiated wild-type recipient mice were infused with 2 × 10^6 BM cells of the indicated genotype and analyzed at 4 mo after transplantation. Data were normalized relative to wild type and are shown as the mean ± SD (BM LSK cells, n = 12; splenic LSK cells, n = 6; CMPs, GMPs, and MEPs, n = 5; *, P < 0.05; **; P < 0.01; ***, P < 0.001). (C) Survival curve of the wild-type recipient mice repopulated by BM cells from indicated mutant mice. The data from four independent experiments were combined (wild type, n = 12; *Ink4a-Arf*$^{-/-}$, n = 11; *Bmi1*$^{-/-}$*Ink4a-Arf*$^{-/-}$, n = 14). The significance of the difference in survival curves was calculated by log-rank test. *, P = 0.0007. (D) PB analysis of white blood cells (WBC), platelets (PLT), and hemoglobin (HGB) of the wild-type recipient mice in C. Data are shown as the mean ± SD. *, P < 0.05; **, P < 0.01; ***, P < 0.001.

Published February 20, 2012

control BM cells (Fig. 1 A). To evaluate the repopulating capacity of *Bmi1*$^{-/-}$*Ink4a-Arf*$^{-/-}$ BM cells precisely, we then transplanted wild-type, *Ink4a-Arf*$^{-/-}$, and *Bmi1*$^{-/-}$*Ink4a-Arf*$^{-/-}$ BM cells into lethally irradiated mice without competitor cells. At 4 mo after transplantation, the recipients repopulated with *Bmi1*$^{-/-}$*Ink4a-Arf*$^{-/-}$ donor cells had significantly fewer lineage marker-negative (Lineage$^-$) Sca-1$^+$ c-Kit$^+$ (LSK) cells in BM than did the control recipients as we reported previously (Oguro et al., 2010; Fig. 1 B). However, they had twofold more megakaryocyte/erythroid progenitors (MEPs) than the controls (Fig. 1 B) and showed extramedullary hematopoiesis as evident from a significant increase in the number of LSK HSCs/multipotent progenitors (MPPs) in spleen (Fig. 1 B). All of the recipient mice repopulated with *Ink4a-Arf*$^{-/-}$ BM cells eventually developed sarcomas or lymphomas and died by 11 mo after transplant, as reported with the *Ink4a-Arf*$^{-/-}$ mice (Fig. 1 C; Serrano et al., 1996). Alternatively, the recipient mice repopulated with *Bmi1*$^{-/-}$*Ink4a-Arf*$^{-/-}$ BM cells died much earlier than the *Ink4a-Arf*$^{-/-}$ controls (Fig. 1 C) and displayed a more progressive thrombocytopenia (Fig. 1 D).

Bmi1-deficient hematopoietic cells induce lethal myelofibrosis

The recipient mice repopulated by *Bmi1*$^{-/-}$*Ink4a-Arf*$^{-/-}$ BM cells had marked hepatosplenomegaly (not depicted) and hypoplastic BM with severe fibrosis (Fig. 2, A and B) at their

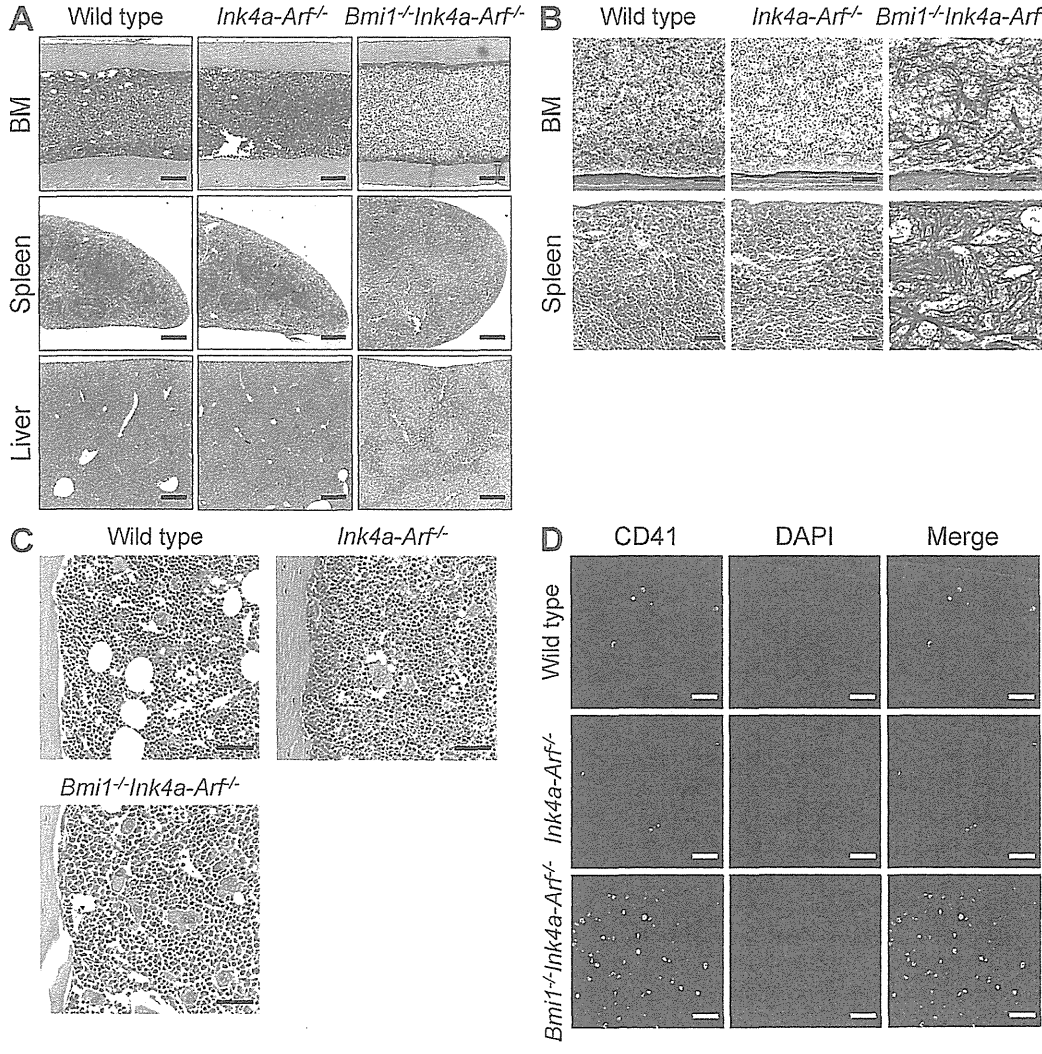

Figure 2. Enhanced megakaryocytopoiesis and massive myelofibrosis induced by *Bmi1*$^{-/-}$*Ink4a-Arf*$^{-/-}$ hematopoietic cells. (A) Hematoxylin and eosin (H&E) staining of BM, spleen, and liver sections. BM, spleen, and liver of representative wild-type recipient mice repopulated by 2 × 10^6 BM cells of the indicated genotype were analyzed at 174 d after transplantation. Bars: 125 µm (BM); 500 µm (spleen and liver). (B) Silver staining of BM and spleen sections in A. Bars, 50 µm. (C) H&E staining of BM sections of representative recipient mice repopulated with the indicated mutant BM cells analyzed at 138 d after transplantation. Bars, 50 µm. (D) CD41 (green) and DAPI (blue) staining of spleen sections of representative recipient mice repopulated with indicated mutant BM cells analyzed at 138 d after transplantation. Bars, 125 µm.

Published February 20, 2012

terminal stage. The spleen structure was destroyed by extramedullary hematopoiesis accompanied by massive fibrosis (Fig. 2, A and B). Extramedullary hematopoiesis was also evident in the liver (Fig. 2 A). All these features resemble those of human primary myelofibrosis (PMF). Notably, the recipient mice infused with *Bmi1*$^{-/-}$*Ink4a-Arf*$^{-/-}$ BM cells along with competitor cells in Fig. 1 A also developed lethal myelofibrosis in a similar fashion (not depicted).

PMF is the rarest and most severe chronic MPN (Tefferi et al., 2007; Levine and Gilliland, 2008). Abnormal megakaryocytosis in the BM has been proposed as the main causative factor for myelofibrosis. Deregulated stem cell signaling, resulting in part from mutated JAK2 and MPL, likely cause abnormal megakaryocytosis. Myelofibrosis is thought to be the consequence of an excessive release/leakage of growth factors within the BM by cells from pathological hematopoietic clones, especially by necrotic megakaryocytes. TGF-β1 is speculated to be one of the major causative growth factors that activate mesenchymal cells (Martyré *et al,* 1994). Although abnormal megakaryocytosis was obscure in BM and spleen because of severe fibrosis at the terminal stage of the disease, the mice at earlier time points after transplantation had marked megakaryocytosis in both BM and spleen (Fig. 2, C and D). These findings clearly implicate pathological megakaryocytosis in the development of lethal myelofibrosis, and indicate that lethal myelofibrosis induced by *Bmi1*$^{-/-}$*Ink4a-Arf*$^{-/-}$ hematopoietic cells follows the natural course of human PMF.

Derepression of *Hmga2* in *Bmi1*-deficient hematopoietic stem/progenitor cells

To identify the genes responsible for PMF-like disease in the absence of Bmi1, we compared gene expression profiles of LSK HSCs/MPPs and common myeloid progenitors (CMPs). In total, 245 and 286 genes were derepressed by more than twofold, specifically in *Bmi1*$^{-/-}$*Ink4a-Arf*$^{-/-}$ LSKs and CMPs, respectively (Fig. 3 A). We then compared the list of derepressed genes with a list of PMF-associated genes identified by gene expression profiling of CD34^{+} cells in human PMF patients (Guglielmelli et al., 2007). *Hmga2* appeared to be commonly up-regulated in *Bmi1*$^{-/-}$*Ink4a-Arf*$^{-/-}$ CMPs and PMF CD34^{+} cells. *HMGA2* was found to be one of eight genes that can distinguish PMF CD34^{+} cells from normal CD34^{+} cells, and abnormal expression of *HMGA2* was associated with the presence of *JAK2*^{V617F} (Guglielmelli et al., 2007). Moreover, overexpression of *HMGA2* was reported in 12 of 12 patients with myelofibrosis with myeloid metaplasia, among which two patients had a chromosomal translocation involving the *HMGA2* gene at 12q (Andrieux et al., 2004). We therefore focused on *Hmga2*. *Hmga2* expression was up-regulated by 1.6- and 13.4-fold in *Bmi1*$^{-/-}$*Ink4a-Arf*$^{-/-}$ LSKs and CMPs, respectively, in our microarray analysis (Fig. 3 A). We then quantified the *Hmga2* expression in each progenitor fraction by quantitative RT-PCR. Because the BM environment of *Bmi1*$^{-/-}$ and *Bmi1*$^{-/-}$*Ink4a-Arf*$^{-/-}$ mice is defective in supporting HSCs (Oguro et al., 2006), we purified progenitors from wild-type recipient BM reconstituted with wild-type, *Ink4a-Arf*$^{-/-}$, or *Bmi1*$^{-/-}$*Ink4a-Arf*$^{-/-}$ BM cells to exclude any environmental effects. *Hmga2* expression was predominantly found in CMPs in wild-type mice, but in the absence of Bmi1, it was derepressed in Flt3^{-}LSK HSCs/MPPs (2.4-fold compared with *Ink4a-Arf*$^{-/-}$ cells) and markedly increased in myeloid-committed progenitors (CMPs, 14.1-fold; granulocyte/macrophage progenitors [GMPs], 268-fold; MEPs, 11.5-fold), but was barely affected in Flt3^{+}LSK lymphoid-primed MPPs (LMPPs, 0.9-fold) or common lymphoid progenitors (CLPs, 0.74-fold; Fig. 3 B). To confirm that this derepression is in fact mediated by loss of Bmi1, we performed RT-PCR analysis on Lineage^{-}c-Kit^{+} *Bmi1*$^{-/-}$ progenitors and found that *Hmga2*, as well as the canonical targets *Ink4a* and *Arf*, are derepressed in a *Bmi1*-deficient setting (Fig. 3 C). These results suggest that Bmi1 functions in the silencing of *Hmga2* in cell types ranging from HSCs to myeloid progenitors.

Direct repression of *Hmga2* transcription by Bmi1

The high-mobility group A (HMGA) nonhistone chromatin proteins alter chromatin structure, and thereby regulate transcription. HMGA proteins have been implicated in both benign and malignant tumors through mechanisms that result in HMGA overexpression. Chromosomal rearrangements involving the region 12q13-15, in which the *HMGA2* gene is located, are one of the major mechanisms causing deregulation of the *HMGA2* gene, giving rise to a truncated transcript lacking the C-terminal tail and/or 3′-UTR. Expression of *HMGA2* is negatively regulated by the let-7 family of microRNAs, which bind to the 3′-UTR of *HMGA2* and restrict its expression. Thus, chromosomal rearrangements within the *HMGA2* locus cause overexpression of a full-length or truncated HMGA2 with a preserved DNA-binding capacity (Fusco and Fedele, 2007; Young and Narita, 2007).

To examine whether Bmi1 directly represses transcription of *Hmga2*, we next characterized the *Hmga2* promoter by conducting chromatin immunoprecipitation (ChIP) assays. To obtain enough cells, we used BM Lineage^{-}c-Kit^{+} progenitors depleted of cells committed to the lymphoid, myeloid, and erythroid lineages. Binding of Bmi1 to the *Hmga2* promoter was detected, but not to the promoter of the control gene, β-*actin* (Fig. 3 D), which was marked with H3K4me3, an active histone mark (not depicted). PRC1 catalyzes the monoubiquitination of histone H2A (H2Aub1) at lysine 119. The *Hmga2* promoter was marked with H2Aub1 in wild-type BM Lineage^{-}c-Kit^{+} progenitors (Fig. 3 D). The levels of Bmi1 binding and H2Aub were significantly reduced in *Bmi1*$^{-/-}$*Ink4a-Arf*$^{-/-}$ Lineage^{-} progenitors compared with the levels in wild-type cells (Fig. 3 E). These results indicate that Bmi1 directly represses the expression of *Hmga2* by marking its promoter with a repressive histone mark.

Hmga2 promotes expansion of progenitor cells and enhances megakaryocytopoiesis in vitro

The specific up-regulation of *HMGA2* expression in PMF, but not in other chronic MPNs, such as polycythemia vera